Cell Reports
Medicine

Article

Opantimirs: A class of antagonizing microRNAs that upregulate Opa1 and improve mitochondrial and disuse myopathies

Graphical abstract

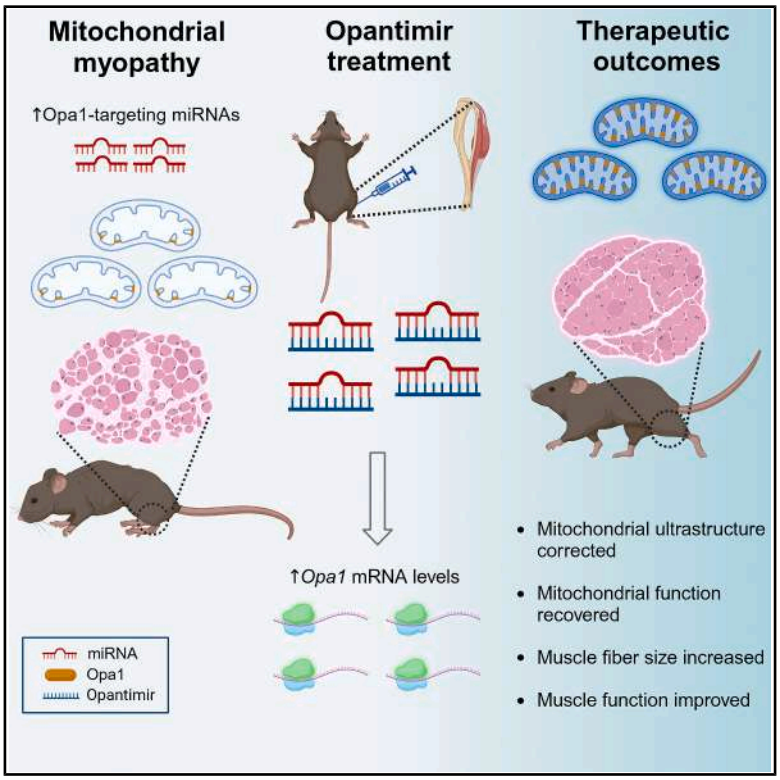

Highlights

- Conserved miR-148/152-3p and miR-128-3p families bind OPA1 3 UTR to lower OPA1
- Opantimirs block these miRNAs, restoring mitochondrial structure via OPA1 upregulation
- Opantimirs-148a/152 rescue mitochondrial shape and function in patient cells
- Opantimirs boost muscle fiber size and strength in Cox15-null and denervation mouse models

Authors

Andre Djalalvandi, Keisuke Takeda, Francesca Grespi, ..., Bert Blaauw, Carlo Viscomi, Luca Scorrano

Correspondence

luca.scorrano@unipd.it

In brief

Djalalvandi et al. show that blockers of Opa1-targeting microRNAs found upregulated in diseased skeletal muscle can restore mitochondrial architecture and muscle performance in mitochondrial myopathy models. This RNA-based therapy revives crista shape to combat mitochondrial myopathies.

Djalalvandi et al., 2025, Cell Reports Medicine 6, 102248
August 19, 2025
https://doi.org/10.1016/j.xcrm.2025.102248

CellPress

Cell Reports Medicine

CellPress
OPEN ACCESS

Article

Opantimirs: A class of antagonizing microRNAs that upregulate Opa1 and improve mitochondrial and disuse myopathies

Andre Djalalvandi,[1,2,7] Keisuke Takeda,[1,2] Francesca Grespi,[1,2] Hualin Fan,[1,2] Tiago Branco Fonseca,[1,2] Leonardo Nogara,[2,3,4] Saman Sharifi,[2,5] Carlotta Barison,[1,2] Martina Semenzato,[1,2] Akiko Omori,[1,2] Raffaele Cerutti,[2,3] Davide Steffan,[2,3] Lorenza Tsansizi,[1,2] Valeria Balmaceda,[1,2] Lukas Alan,[1,2] Camilla Bean,[6] Bert Blaauw,[2,3] Carlo Viscomi,[2,3] and Luca Scorrano[1,2,7,*]

[1]Department of Biology, University of Padova, Via U. Bassi 58B, 35121 Padova, Italy
[2]Veneto Institute of Molecular Medicine, Via Orus 2, 35129 Padova, Italy
[3]Department of Biomedical Sciences University of Padova, Via U. Bassi 58B, 35121 Padova, Italy
[4]Department of Pharmaceutical Sciences, University of Padova, Via Marzolo, 5 35131 Padova, Italy
[5]Department of Medicine, University of Padova, Via Giustininani 1, 35128 Padova, Italy
[6]Department of Medical Sciences, University of Udine, Via Colugna 50, 33100 Udine, Italy
[7]Lead contact
*Correspondence: luca.scorrano@unipd.it
https://doi.org/10.1016/j.xcrm.2025.102248

SUMMARY

Alterations in mitochondrial ultrastructure and reduced levels of the crista-shaping protein Opa1 are key features of mitochondrial myopathies and aging. We identify and characterize a biological therapy that improves mitochondrial and disuse myopathy models by boosting Opa1 levels. *In silico* analysis identifies microRNAs (miRNAs) 128-3p and 148/152-3p family as conserved modulators of *OPA1* transcription and elevated in various muscle disorders. These miRNAs target the 3′ UTR of murine and human *OPA1*, reducing its mRNA and protein levels, causing mitochondrial fragmentation and crista disorganization. Genetic experiments confirm that their mitochondrial effects rely on 3′ UTR binding. In mitochondrial disease patient cells and murine models, elevated OPA1-specific miRNA levels are reduced by antagonistic miRNAs (Opantimirs), which restore mitochondrial ultrastructure, morphology, and function. *In vivo*, Opantimirs correct mitochondrial ultrastructure and fiber size in muscles of denervated and Cox15-ablated mice, improving strength in the latter. Thus, biopharmacological correction of the mitochondrial ultrastructure can ameliorate mitochondrial myopathies.

INTRODUCTION

Mitochondrial diseases are a group of clinically heterogeneous conditions that arise from oxidative phosphorylation (OXPHOS) malfunction due to defects in respiratory chain complexes.[1] These disorders affect one in every 2,000 individuals, can manifest in infancy or adulthood, and are caused by pathogenic mutations in either nuclear DNA or mitochondrial DNA (mtDNA).[2] Biochemically, complex I and complex IV deficiencies are the most frequent causes of faulty mitochondrial bioenergetics in mitochondrial diseases.[3] Organs that heavily rely on oxidative metabolism such as muscle, brain, heart, and kidney are particularly susceptible to becoming pathological.[1,2] Mitochondrial myopathies are a subset of mitochondrial syndromes hallmarked by pronounced defects in skeletal muscle. Clinical features commonly reported in mitochondrial myopathy patients include progressive muscle atrophy and weakness, motor impairments, exercise intolerance, and fatigue.[4] Despite a nutrient intervention showing promise in clinical trials for adult-onset mitochondrial myopathy,[5] there are currently no approved therapies, highlighting the need to develop novel curative interventions to combat these disorders.

Distorted cristae shape is a pathological hallmark of mitochondrial myopathy. Hence, restoring the ultrastructure of mitochondria could serve as an effective therapeutic strategy.[6] Mitochondrial shape and ultrastructure are controlled by a set of large dynamin-related guanosine-5′-triphosphatase (GTPase) proteins that modulate fusion, fission, and cristae remodeling.[7] Mitofusin (MFN) 1 and 2 mediate outer mitochondrial membrane fusion. Optic atrophy 1 (OPA1) controls inner mitochondrial membrane fusion and crista remodeling, whereas Dynamin-related protein 1 coordinates mitochondrial fission.[8,9] These mitochondria-shaping proteins are crucial for maintaining skeletal muscle homeostasis.[10] Notably, muscle-specific deletion of OPA1 in adult mice induces a myopathic phenotype more severe than double MFN1/MFN2 deletion.[11] Conversely, mice where OPA1 levels are genetically upregulated are protected against denervation-induced muscle atrophy[12] and primary OXPHOS

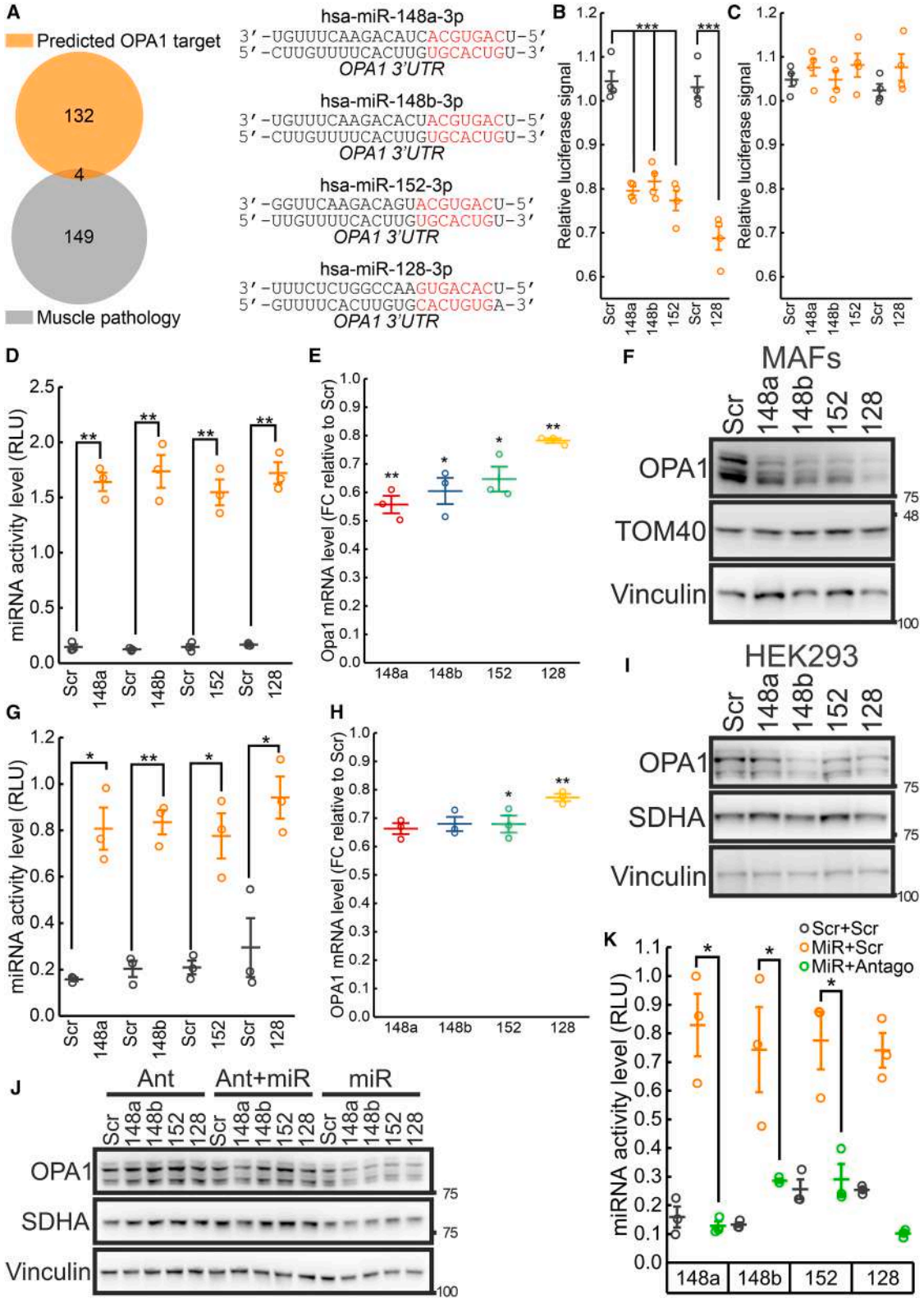

(legend on next page)

deficiency. In particular, OPA1 overexpression ameliorates the myopathic phenotype caused by the ablation of the cytochrome *c* oxidase assembly factor Cox15 (cytochrome c oxidase assembly homolog 15) in the skeletal muscle,[13] suggesting that correction of mitochondrial ultrastructure by increased OPA1 levels can be exploited to treat mitochondrial myopathies. On the other hand, in the *Opa1* transgenic mouse model, OPA1 is overexpressed ubiquitously and also during development. It is therefore unclear whether upregulation of Opa1 after development can produce the same curative effects. Moreover, a therapeutic intervention involving *OPA1* upregulation appears challenging because of potential off-target effects in unaffected tissues. A more appropriate therapeutic strategy for myopathies with reduced *OPA1* transcript levels shall increase OPA1 levels only in the affected muscle tissue. We therefore sought to identify factors that modulate *OPA1* transcript levels in diseased muscles and to target them.

Here, we report the identification of four *OPA1*-targeting microRNAs (miRNAs), small non-coding RNAs (~22 nt long) involved in gene regulation,[14] that are increased in myopathy. Leveraging miRNA antagonizers (AntimiRs), a class of chemically engineered oligonucleotides that base-pair with miRNAs and inhibit their silencing action on mRNA,[15,16] we developed *OPA1* AntimiRs (Opantimirs) that efficaciously inhibit *OPA1*-targeting miRNAs and increase OPA1 levels in cells and *in vivo*. Delivery of Opantimirs ameliorates mitochondrial ultrastructure and function in mitochondrial disorder patient cells and curtails mitochondrial and disuse myopathy.

RESULTS

Opa1 expression is directly modulated by the miR-148/152 family and miR-128

To identify miRNAs that might regulate Opa1 expression in mitochondrial myopathies, we used the TargetScan, miRWalk, and miRDB search engines to ascertain *in silico* evolutionarily conserved miRNAs predicted to target *OPA1* with high binding affinity. We then integrated this dataset with the list of miRNAs upregulated in muscle pathology extracted from the miRNA sequencing data of atrophic mouse muscle (GSE51648),[17] from the Human microRNA Disease Database[18] (HMDD, http://www.cuilab.cn/hmdd) miRNA profile of muscular dystrophy patients and from miRNA expression datasets of muscle biopsies from various muscle disorders.[19] The Venn diagram of the overlapping hits contained miR-148a-3p, miR-148b-3p, miR-152-3p (miR-148/152-3p family), and miR-128-3p as both predicted OPA1-targeting and upregulated in muscle disease (Figure 1A).

To determine whether miR-148/152-3p and miR-128-3p specifically targeted OPA1, we exploited the firefly luciferase (fLuc)-based reporter assay by generating sensors containing the *OPA1* 3 UTR fragment with the seed site for miR-148/152-3p family and for miR-128-3p coupled to the fLuc cDNA. Because of the presence of a Renilla control coexpressed by the same plasmid, we could calculate the ratio of the reduction in the fLuc luminescence occurring when a miRNA bound to its *OPA1* seed sequence (destabilizing the fLuc mRNA) to the reference Renilla luminescence. The miR-148/152-3p or miR-128-3p mimics reduced the fLuc/Renilla luminescence ratio, indicating that these miRNAs target the respective *OPA1* 3 UTR fragment to which they were predicted to bind and degrade the mRNA carrying this 3 UTR (Figure 1B). Site-directed mutagenesis was used to introduce three point mutations at the putative target sites in the *OPA1* 3 UTR constructs, which served as a negative control. The effect of miR-148/152-3p and miR-128-3p activity on *OPA1* 3 UTR degradation was negated in the *OPA1* 3 UTR-mutant plasmid, revealing that these miRNAs directly interact with the *OPA1* 3 UTR at the predicted binding sites (Figure 1C). We then generated ratiometric miRNA sensors containing a 2-repeat sequence of miRNA seed sequence linked to a fLuc-based reporter to measure the functional activity of miRNAs. In all cases, miRNA overexpression reduced the fLuc luminescence in mouse adult fibroblasts (MAFs) (Figure 1D) and in human embryonic kidney 293 (HEK293) cells (Figure 1G). These results indicated that the designed miRNAs were successfully delivered and targeted their seed sequence in mouse and human cells. Next, we measured *OPA1* mRNA and protein content in cells where we overexpressed each miRNA. Levels of *OPA1* mRNA (Figure 1E) and protein (Figure 1F) were reduced in mouse and human cells that overexpressed miR-148/152-3p and miR-128-3p (Figures 1H and 1I), suggesting that these miRNAs effectively regulate *OPA1*

Figure 1. MiR-148/152 family and miR-128 specifically target *OPA1* 3 UTR to control its expression in mouse and human

(A) Venn diagram of miRNA expression profiles from human and mouse muscle pathology datasets and miRNA predicted to regulate the OPA1 3 UTR using prediction search engines (left). The region of human *OPA1* 3 UTR containing the predicted seed sequence (red) for miR-148a, 148b, 152, and 128 is aligned with the respective miRNA (left).

(B) MAFs expressing the ratiometric luminescence Opa1 3 UTR-miRNAs binding reporters were transfected with 30 nM of the indicated miRNA for 24 h. Average ± SEM of 4 biological replicate experiments of anti-Opa1 3 UTR miRNA activity. ***$p < 0.001$ in a Student's unpaired t test.

(C) Experiments were as in (B) except that the OPA1 3 UTR contained three point mutations in the binding sequence for the respective miRNA.

(D) MAFs expressing the ratiometric luminescence miRNA activity reporters were transfected with 30 nM of the indicated miRNA for 24 h. Average ± SEM of 3 biological replicate experiments of activity of the indicated miRNAs. **$p < 0.01$ in a Student's unpaired t test.

(E) Average ± SEM from 3 biological replicate experiments of *Opa1* mRNA expression levels quantified by reverse-transcription PCR (RT-PCR) in MAFs transfected for 24 h as indicated. *$p < 0.05$ and **$p < 0.01$ in a Student's unpaired t test.

(F) Representative immunoblots of MAFs transfected as indicated. After 48 h, cells were lysed, and equal amounts of lysates (20 μg) were separated by SDS-PAGE and immunoblotted using the indicated antibodies.

(G–I) Experiments were performed as in (D), (E), and (F), respectively, except that HEK293 cells were used.

(J) Representative immunoblots of MAFs transfected as indicated. After 72 h, cells were lysed and equal amounts of lysates (20 μg) were separated by SDS-PAGE and immunoblotted using the indicated antibodies.

(K) Experiments were as in (D) except that, following transfection with the indicated miRNA for 24 h, MAFs were transfected also with the indicated AntagomiR for 24 h. *$p < 0.05$ in a Student's unpaired t test.

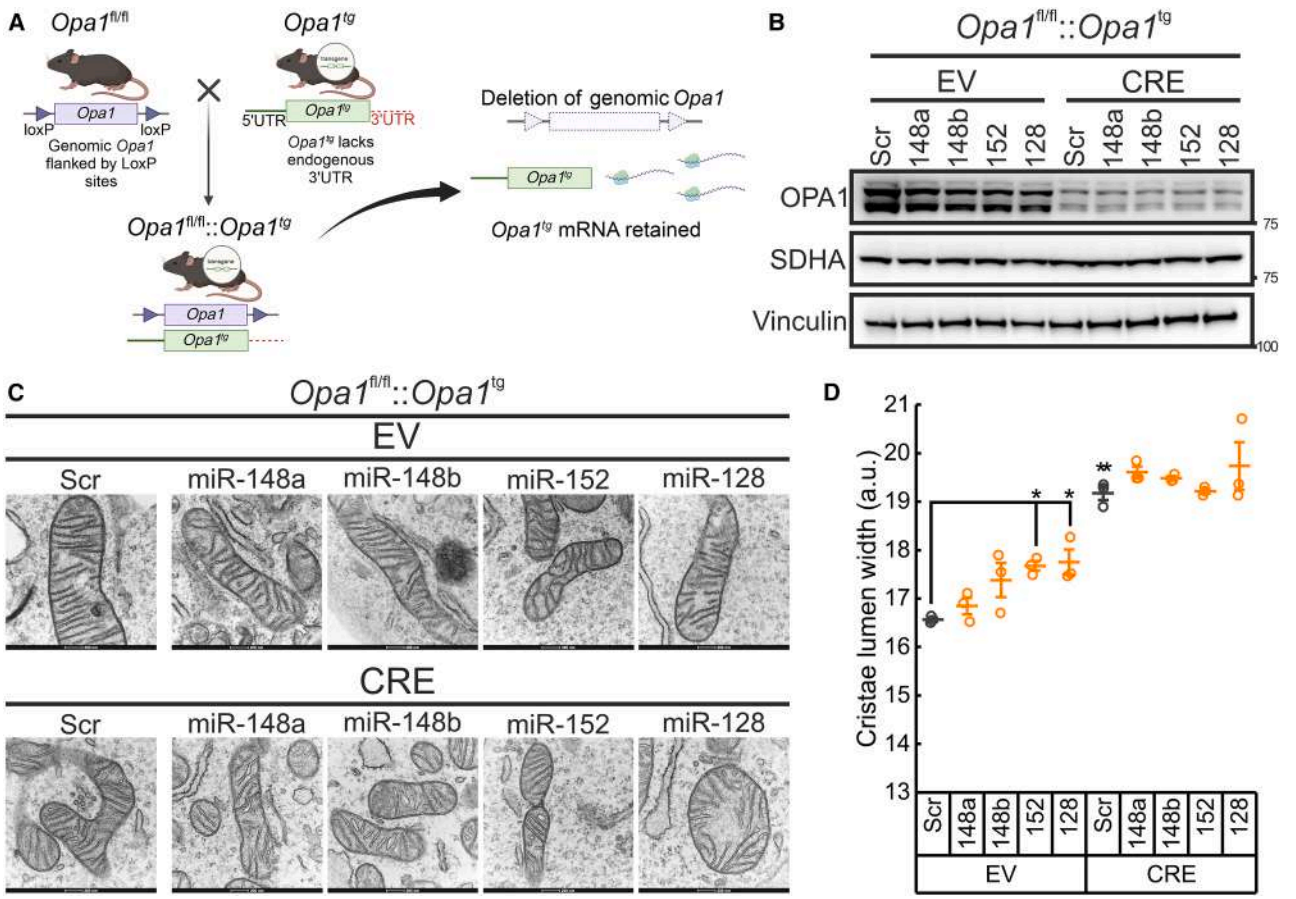

Figure 2. MiR-148/152 and miR-128 require genomic OPA1 to modulate crista structure

(A) Schematic representation of *Opa1*$^{fl/fl}$ and *Opa1*^{tg} mouse breeding to generate *Opa1*$^{fl/fl}$::*Opa1*^{tg} mice.

(B) Representative immunoblots of the indicated MAFs infected for 72 h with the indicated adenovirus. After 72 h, cells were transfected with the indicated miR, and after 48 h, cells were lysed and equal amounts of lysates (20 μg) were separated by SDS-PAGE and immunoblotted using the indicated antibodies.

(C) Representative electron micrographs from experiments as in (B). Scale bar, 200 nm.

(D) Average ± SEM of crista lumen width from 3 biological replicate experiments as in (C) (n = 100–120 mitochondria per condition, 3 cristae per mitochondrion). $^{*}p < 0.05$ and $^{***}p < 0.001$ in a one-way ANOVA.

expression in mammals. Notably, protein levels of other major regulators of mitochondrial dynamics were unaltered from miRNA overexpression (Figures S1A and S1B). We then designed AntimiRs against these OPA1-targeting miRNAs (collectively dubbed Opantimirs) and assessed their ability to counteract the effects of the corresponding miRNAs and stabilize OPA1 levels. Indeed, while OPA1 levels were reduced by miRNA expression, co-transfection with their respective Opantimirs abolished the effects of the miRNAs and fully stabilized OPA1 (Figure 1J). By using miRNA-based sensors, we also verified that Opantimirs inhibited the miRNAs they were designed to target (Figure 1K). Altogether, these experiments establish OPA1 as a target of the miR-148/152-3p family and miR-128-3p.

The miR-148/152 family and miR-128 regulate mitochondrial ultrastructure through an Opa1-dependent pathway

We next investigated whether the identified miRNAs exerted biological effects on mitochondrial shape and ultrastructure through OPA1 modulation. Confocal images and transmission electron microscopy (TEM) analysis of cells overexpressing the four miRNAs displayed more fragmented mitochondria with fewer cristae (Figures S2A–S2E). To delineate whether this effect on mitochondrial shape and ultrastructure was specifically dependent on *OPA1* transcript regulation, we generated *Opa1*$^{fl/fl}$::*Opa1*^{tg} mice[20] and we extracted *Opa1*$^{fl/fl}$::*Opa1*^{tg} MAFs. In these cells, genomic *Opa1* alleles are flanked by *loxP* sites, and an additional *Opa1* transgene (*Opa1*^{tg}) is inserted into the hypoxanthine phosphoribosyltransferase (HPRT) locus on the X chromosome. Notably, the *Opa1*^{tg} mRNA lacks the endogenous 3 UTR to which miRNAs bind, rendering the transcript insensitive to miRNA-mediated degradation (Figure 2A). Cells were treated with Cre recombinase (Cre) lentivirus for 72 h to eliminate genomic-encoded OPA1 protein, followed by miRNA transfection for 48 h. Immunoblotting analysis showed that OPA1 protein levels remained unchanged after miRNA overexpression compared to scramble treatment (Figure 2B). Moreover, cristae integrity was

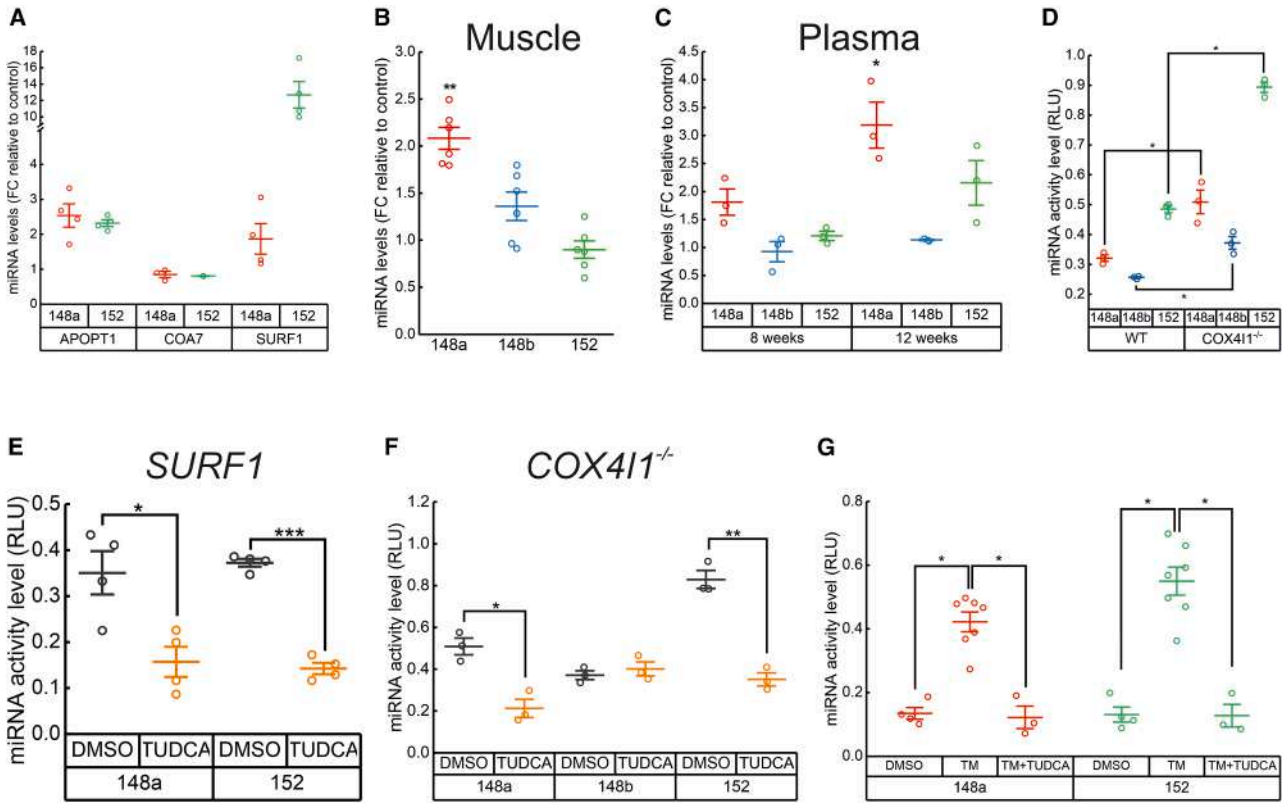

Figure 3. MiR-148a and miR-152 accumulate in models of mitochondrial myopathy and upon ER stress induction

(A) Average ± SEM of 4 biological replicate experiments of reverse-transcription PCR (RT-PCR) of the indicated miRNA levels in fibroblasts from patients with mutations in the specified gene, compared to healthy controls. *** < 0.001 and ****$p < 0.0001$ in a Student's unpaired t test.

(B and C) Average ± SEM of 3 (plasma) or 6 (muscle) biological replicates of RT-PCR for the indicated miRNA levels in muscles and plasma isolated from *Cox15*$^{sm/sm}$ mice of the indicated age compared to wild-type mice. In the case of muscle, mice were 8 weeks old. *$p < 0.05$ and **$p < 0.01$ in a Student's unpaired t test.

(D) Cells of the indicated genotype were transfected with the indicated ratiometric luminescence miRNA activity reporters, and after 24 h activity of the indicated miRNAs was measured. Data show average ± SEM of 3 biological replicates. *$p < 0.05$ in a one-way ANOVA.

(E and F) *SURF1* patient fibroblasts and COX4I1-deleted HEK293 cells were transfected with the indicated ratiometric luminescence miRNA activity reporters and after 24 h treated where indicated with tauroursodeoxycholic acid (TUDCA, 200 μM) for 6 h. Data show average ± SEM of 3 independent experiments of activity of the indicated miRNAs. **$p < 0.01$ in a one-way ANOVA.

(G) C2C12 myotubes were transfected with the indicated ratiometric luminescence miRNA activity reporters and after 24 h treated where indicated with tunicamycin (TM, 1 μg/mL) for 24 h or with TM and 200 μM TUDCA for further 24 h. Data show average ± SEM of 3–7 biological replicate experiments of activity of the indicated miRNAs. *$p < 0.05$ in a one-way ANOVA.

preserved, with no significant differences in cristae lumen width (CLW) (Figures 2C and 2D). These results imply that miRNAs do not affect cristae shape when genomic *Opa1* is absent, indicating that their impact on cristae morphology is mediated through regulation of expression of *Opa1* from its genomic locus.

Elevated miR-148a and miR-152 levels in mitochondrial myopathy patient cells and mouse models

Since the miR-148/152-3p family and miR-128-3p were reported to accumulate in primary muscle diseases,[19,21] we investigated whether these miRNAs were increased in mitochondrial myopathies. We measured expression levels of miRNAs in skin fibroblasts from three mitochondrial myopathy patients characterized by cytochrome c oxidase (COX) deficiency harboring mutations in genes encoding COX assembly factors. The mutant alleles included Surfeit locus protein 1 (*SURF1*), cytochrome *c* Oxidase Assembly Factor 7 (*COA7*), and Apoptogenic protein 1 (*APOPT1*) that cause Leigh syndrome,[22,23] mitochondrial leukoencephalopathy,[24] and mitochondrial encephalomyopathy,[25] respectively. Levels of miR-148a-3p and miR-152-3p were ∼2.5-fold higher in *APOPT1* patient cells compared to healthy control fibroblasts (Figure 3A). *SURF1* patient cells exhibited ∼13-fold higher miR-152-3p levels and elevated miR-148a-3p levels (Figure 3A), whereas miR-148a-3p and miR-152-3p levels remained unchanged in *COA7* cells (Figure 3A). The discrepancies in miRNA content between mitochondrial myopathy patients could be attributed to varying levels of residual COX activity (12% in *SURF1* versus 33% in *COA7*).

We next tested whether these miRNAs are increased in mitochondrial myopathy muscle tissue and blood. We capitalized on the Cox15 skeletal-muscle-specific knockout (KO) (*Cox15*$^{sm/sm}$) mouse that manifests an early-onset progressive mitochondrial myopathy.[26] Cox15 is a COX assembly factor and is a key enzyme in the biosynthesis of heme A. Mutations in *COX15* cause cardiomyopathy, encephalopathy, and Leigh syndrome in infants.[27–29] In 8-week-old *Cox15*$^{sm/sm}$ gastrocnemius, miR-148a-3p levels were increased (Figure 3B). Additionally, we found that plasma miRNA levels in *Cox15*$^{sm/sm}$ mice were elevated at 12 weeks (Figure 3C), suggesting that these miRNAs are secreted into the bloodstream. Altogether, these data indicate that induction of these miRNAs is a conserved mammalian response to COX deficiency. We next evaluated another myopathy mouse model where muscle wasting was induced by denervation via surgical sciatic nerve resection.[12] Two weeks post-surgery, we measured the accumulation of miR-148a-3p and miR-152-3p transcripts in the gastrocnemius muscle (Figures S3A and S3B). These miRNA levels negatively correlated with OPA1 expression at both mRNA and protein levels (Figures S3C and S3D). Altogether, these results indicate that miR-148a and miR-152 accumulate in cells from Leigh syndrome patients and in mouse models of mitochondrial and disuse myopathy.

Endoplasmic reticulum stress controls miR-148a-3p and miR-152-3p levels upon COX deficiency

Endoplasmic reticulum (ER) stress is a pathological response toward mitochondrial defects in muscle,[11,30,31] and the induction of miRNAs is an often-overlooked component of ER stress.[32] Thus, we checked whether ER stress could be driving the miRNA upregulation in conditions of COX deficiency and myopathy. We used a genetic model of complete COX deficiency utilizing CRISPR-Cas9-deleted *COX4I1* KO HEK293 cells. COX4I1 is an initiator subunit for COX and is mutated in cases of Fanconi anemia and Leigh-like syndrome.[33,34] miR-148a-3p, miR-148b-3p, and miR-152-3p levels were increased in this cell line (Figure 3D). To alleviate ER stress in *SURF1* patient fibroblasts and *COX4I1* KO cells, we administered the chemical chaperone tauroursodeoxycholic acid (TUDCA),[30] which reduced levels of miR-148a-3p and miR-152-3p (Figures 3E and 3F). Next, we induced ER stress in C2C12 myotubes by using the prototypical ER stressor tunicamycin.[35] Tunicamycin increased levels of miR-148a-3p and miR-152-3p, and co-treatment with TUDCA nullified its effects (Figure 3G). Taken together, these results imply that ER stress, a common mitochondrial myopathy trait that is also sensitive to TUDCA,[11,36] can induce miR-148a-3p and miR-152-3p.

MiR-152 inhibition increases OPA1 levels and corrects mitochondrial morphology and ultrastructure in *SURF1* patient cells

Given that miRNAs controlling OPA1 levels were upregulated in mitochondrial myopathy, we sought to understand if blocking miRNA activity could increase OPA1 levels and restore mitochondrial ultrastructure in these disorders. Having already established that Opantimirs effectively inhibit their respective miRNAs (Figure 1I), we tested whether AntimiR-152-3p (Ant-152-3p) treatment could increase OPA1 levels by silencing miR-152-3p in *SURF1* patient cells. Ant-152-3p treatment concentrations at 30, 60, and 90 nM reduced miR-152-3p levels and increased OPA1 protein levels in *SURF1* patient cells (Figures 4A and 4B). To evaluate AntimiR efficacy in regulating OPA1 under OXPHOS-defective conditions in a muscle-specific cell lineage, we treated C2C12 myotubes with the mitochondrial translation inhibitor Actinonin, the uncoupler carbonyl cyanide m-chlorophenyl hydrazone (CCCP) and the ATP synthase inhibitor oligomycin. All three pharmacological treatments resulted in the accumulation of miR-152-3p, CCCP, and oligomycin also reducing OPA1 transcript (Figures S4A and S4B) by significantly engaging the *OPA1* 3 UTR (Figure S4C) via its seed sequence (Figures S4D and S4E). Ant-152-3p effectively inhibited miR-152-3p activity, prevented Opa1 3 UTR decay, and restored Opa1 expression levels in OXPHOS-defective C2C12 cells (Figures S4E–S4G).

Confocal images revealed a restored mitochondrial network in Ant-152-3p-treated *SURF1* cells (Figures 4C and 4D). This rescue effect on mitochondrial morphology was also observed in *SURF1* homozygous mutant, *COA7* and *APOPT1* cell lines (Figures S5A and S5B). TEM analysis showed that Ant-152-3p treatment reduced CLW to levels comparable to control mitochondria (Figures 4E and 4F). Not only did Ant-152-3p treatment enhance OPA1-dependent crista shape but also improved respiratory chain complex stability, evidenced by increased protein content of subunits from respiratory complexes I, III, IV, and V (Figure 4A).

MiR-148a inhibition rescues muscle function in *Cox15*$^{sm/sm}$ mice

As miR-148a-3p levels were found elevated in *Cox15*$^{sm/sm}$ mouse muscle (Figure 3B), we investigated whether AntimiR delivery to inhibit miR-148a-3p could ameliorate the phenotype in these mice. The 2 -0 -O-(2-methoxyethyl) (MOE) AntimiRs used in this study are chemically modified oligonucleotides with enhanced stability and cellular uptake, enabling them to downregulate target miRNAs in multiple organs, including skeletal muscle, for up to 3–4 weeks.[15,37] AntimiR-148a-3p (Ant-148a-3p) was resuspended in PBS at 100 nM concentration and delivered intramuscularly in the gastrocnemius at three distinct sites. Each site received 20 μL, totaling 6 pmol of Ant-148a-3p per mouse, whereas the contralateral leg received a scramble control injection. Treatment began at 6 weeks of age and continued for 4 weeks. We preliminarily confirmed that increasing concentrations of Ant-148a-3p were well tolerated *in vitro* (Figure S6A). Furthermore, counts of erythrocytes, platelets and leukocytes remained within normal ranges, demonstrating that AntimiRs are well tolerated *in vivo* and do not elicit an overt immune response (Figures S6B–S6F). Finally, the treatment regimen did not affect miR-148a-3p levels in the heart, liver, kidney, and spleen, the histology of which also appeared unaltered, indicating minimal or no systemic leakage of Opantimir molecules following intramuscular injection in the gastrocnemius and the lack of major effects in distant organs (Figures S6G and S6H).

Wheat germ agglutinin (WGA) staining of muscle fiber cross sections performed to visualize muscle cross-sectional area

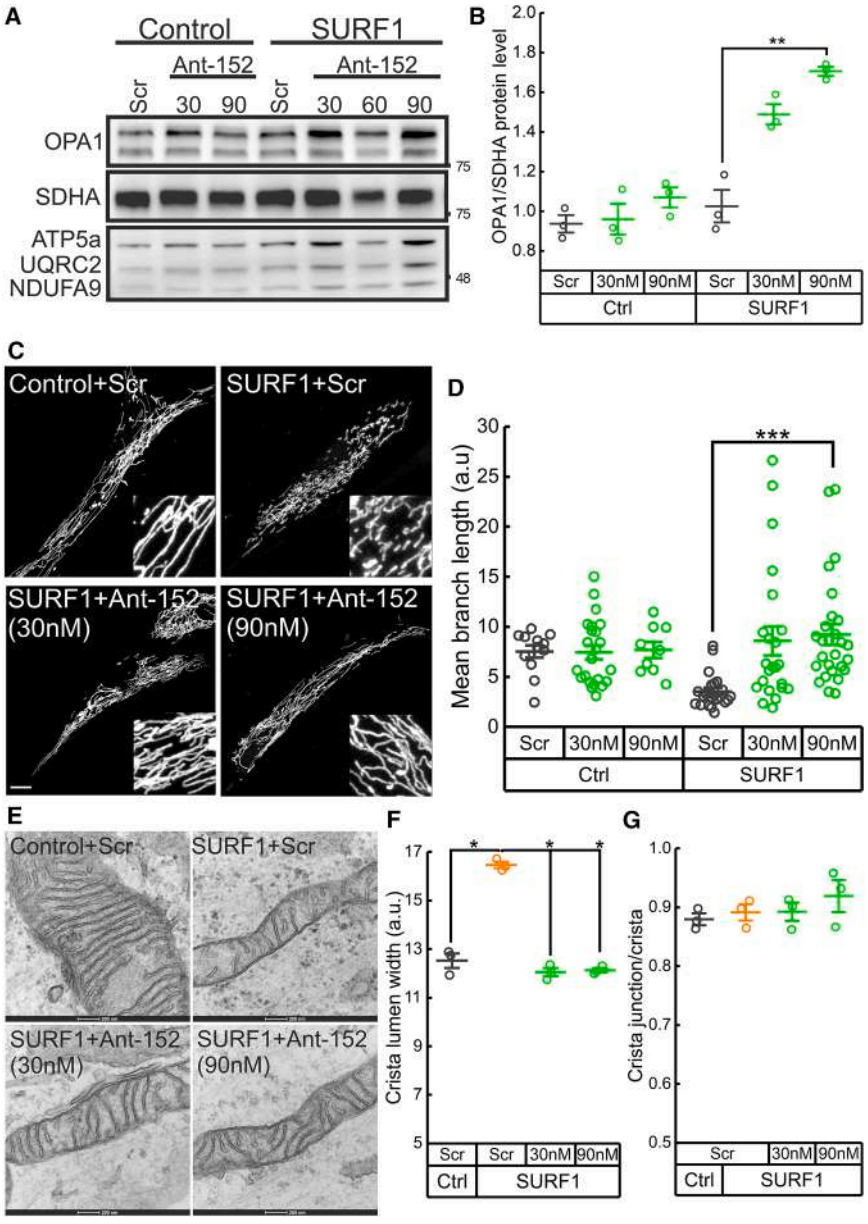

Figure 4. Opantimir152 restores mitochondrial fusion and crista shape in *SURF1* patient cells

(A and B) Representative immunoblots of fibroblasts from healthy controls (left) and *SURF1* patients (right) treated with the indicated concentrations (nM) of Opantimir152 (Ant-152). After 72 h, cells were lysed and equal amounts of proteins (20 μg) were separated by SDS-PAGE and immunoblotted using the indicated antibodies. (B) Average ± SEM of 3 biological replicate experiments as in (A) of Opa1 levels normalized to succinate dehydrogenase complex flavoprotein subunit A (SDHA) by densitometric analysis from *SURF1* patients compared to healthy controls. $^{**}p < 0.01$ in a two-way ANOVA.

(C) Control and *SURF1* patient fibroblasts were transfected as indicated for 24 h and then transfected with a mitochondrially targeted dsRed (mtRFP) for 48 h. After 72 h, cells were fixed and representative confocal images were acquired. Scale bar, 10 μm. The insets represent 3× magnification of the acquired images.

(D) Average ± SEM of mean mitochondrial branch length values from 3 biological replicate experiments as in (D) (n = 13–28 cells per condition). $^{***}p < 0.001$ in a Kruskal-Wallis ANOVA.

(E) Representative electron micrographs from control and *SURF1* patient fibroblasts transfected as indicated for 72 h. Scale bar, 200 nm.

(F and G) Average ± SEM of crista lumen width (F) or of crista junctions/number of cristae (G) from 3 biological replicate experiments as in (E) (n = 100–120 mitochondria per condition, 3 cristae per mitochondrion). $^{***}p < 0.001$ in a one-way ANOVA.

(CSA) indicated that muscle fibers were larger in Ant-148a-3p-treated gastrocnemii compared to scramble-treated muscle (Figures 5A and 5B). At the molecular level, Ant-148a-3p treatment reduced expression levels of the major atrophy-related genes from the ubiquitin proteosome system and autophagy lysosome system (Figure 5F), indicating a suppression of the atrophy program. Muscle function was assessed using a muscle lever system, with maximum muscle force measurements recorded by electrical stimulation of the gastrocnemius muscle. Muscle force was higher in Ant-148a-3p-treated *Cox15*$^{sm/sm}$ muscle compared to scramble-treated muscle (Figure 5C). Collectively, these data reveal that miR-148a-3p silencing through AntimiR delivery can recover muscle size and function in *Cox15*$^{sm/sm}$ mice.

MiR-148 inhibition ameliorates mitochondrial ultrastructure and function in *Cox15* $^{sm/sm}$ mouse

Immunoblot analysis showed increased OPA1 protein levels, and electron micrographs illustrated less crista abnormalities in Ant-148a-3p-treated muscle compared to scramble-treated muscle in *Cox15*$^{sm/sm}$ mice (Figures 6A–6C). Ant-148a-3p-treated Cox15$^{sm/sm}$ muscles displayed higher COX4 protein content (Figure 6A) and a marked recovery of COX-positive fibers (Figure 6D) in histochemical staining. Functional analysis using high-resolution respirometry to measure oxygen consumption on homogenized gastrocnemii revealed increased maximal respiration and respiratory control ratio in Ant-148a-3p-treated mice compared to scramble-treated mice (Figures 6E and 6F), demonstrating improved mitochondrial bioenergetics. These results provide evidence that miR-148a-3p inhibition via antimiR treatment can effectively increase OPA1 levels, stabilize crista shape, and correct mitochondrial function in *Cox15*$^{sm/sm}$ mice.

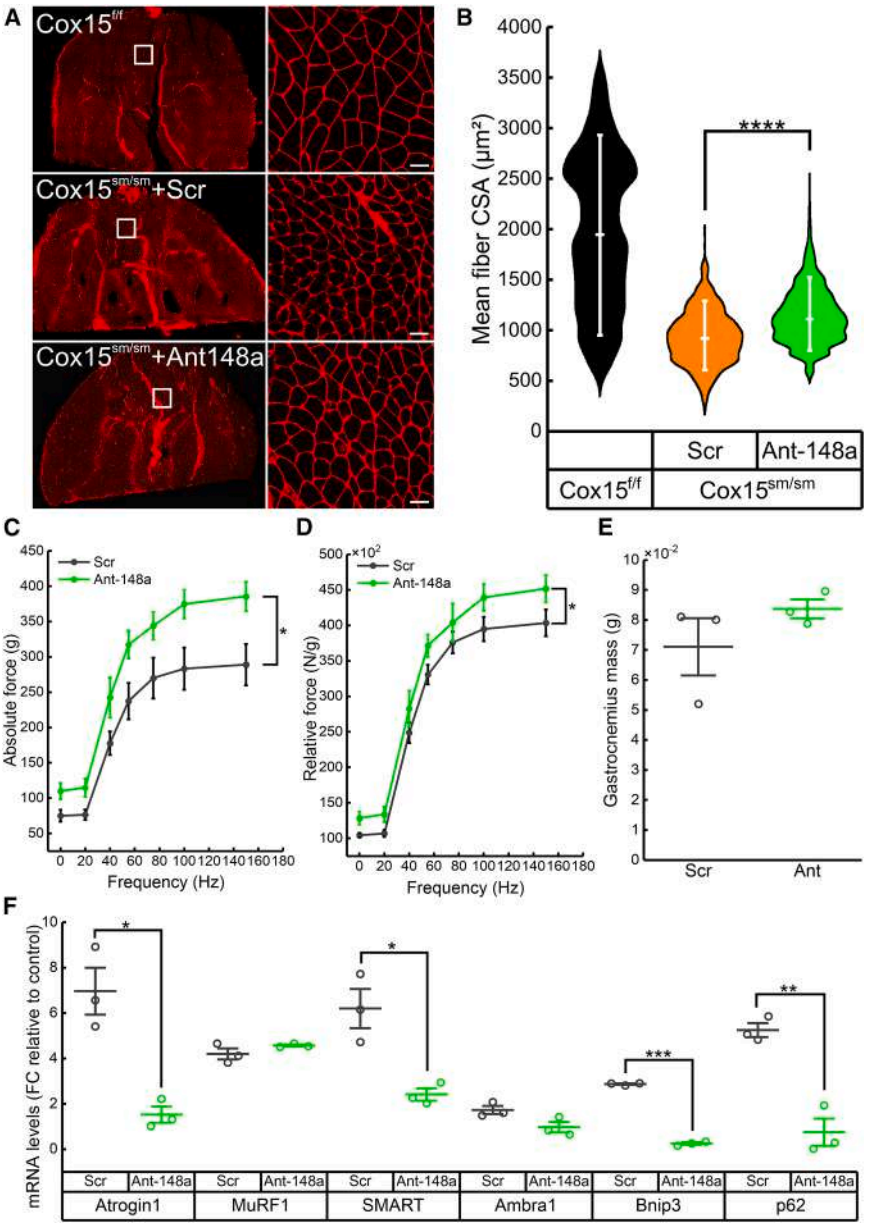

Figure 5. Opantimir148a improves muscle function in *Cox15*$^{sm/sm}$ mice

(A) Representative confocal images of cross sections of WGA-stained gastrocnemii from mice of the indicated genotype treated with the indicated AntagomiR (6 pmol/injection) triweekly for 4 weeks by IM injection at 3 different locations in the gastrocnemius. The boxed area in the whole muscle cross section is enlarged on the right. Scale bar, 50 μm.

(B) Violin plots of fiber cross-sectional area from 3 biological replicate experiments as in (A). Median and 10th and 90th percentiles (whiskers) are shown. ****$p < 0.0001$ in a one-way ANOVA.

(C and D) Average ± SEM of absolute muscle force measurements (C) and of muscle force measurements normalized to muscle mass (D) of gastrocnemii electrically stimulated at the indicated frequencies from three individual *Cox15*$^{sm/sm}$ mice treated as indicated following the same protocol as in (A) ($n = 3$ biological replicates). *$p < 0.05$ in a Kruskal-Wallis ANOVA.

(E) Average ± SEM of three *Cox15*$^{sm/sm}$ gastrocnemii mass treated as indicated following the same protocol as in (A) ($n = 3$ biological replicates).

(F) Average ± SEM of expression levels quantified by RT-PCR of the indicated genes in *Cox15*$^{sm/sm}$ gastrocnemii treated as indicated following the same protocol as in (A) ($N = 3$ biological replicates). *$p < 0.05$, **$p < 0.01$, and ***$p < 0.001$ in a one-way ANOVA.

MiR-148 and miR-152 inhibition rescue muscle atrophy and mitochondrial ultrastructure after denervation

Given that miR-148a-3p and miR-152-3p levels were elevated and OPA1 levels were reduced in denervated muscle (Figure S3), we investigated whether delivering antimiRs could effectively treat this form of muscle atrophy. We administered a mix of antimiRs targeting miR-148a-3p and miR-152-3p at a concentration of 6 pmol triweekly, beginning on day 3 post-surgery. WGA staining of muscle cross sections revealed higher fiber CSA values in antimiR-treated gastrocnemii compared to scramble-treated muscle (Figures 7A and 7B). Additionally, electron micrographs of antimiR-treated muscle showed fewer abnormalities in mitochondria compared to those in scramble-treated mice (Figures 7C and 7D). The antimiR mix effectively inhibited miR-148a-3p and miR-152-3p activity (Figure 7E), and immunoblotting demonstrated a partial restoration of OPA1 protein levels (Figure 7F). These findings suggest that increased OPA1 levels from AntimiR treatment help protect against denervation-induced muscle atrophy. Finally, to ascertain whether the therapeutic effect of AntimiRs on mitochondrial and muscle function in these two models depended on OPA1 regulation, we acutely deleted *Opa1* specifically in skeletal muscle capitalizing on the already established HAS-Cre-ER::*Opa1*$^{fl/fl}$ tamoxifen-inducible muscle-specific mouse line[11] (Figure S7A). The deletion of Opa1 induced miR-148a-3p and miR-152-3p accumulation (Figure S7B) and caused muscle atrophy (Figures S7C and S7D). Treatment with AntimiRs against miR-148a-3p and miR-152-3p silenced these miRNAs but did not impact OPA1 levels, muscle CSA, mitochondrial ultrastructure, or function (Figures S7A–S7I). These findings suggest that the therapeutic benefits of Opantimirs in myopathy are connected to their role in enhancing the Opa1-dependent crista remodeling pathway and do not occur when genomic Opa1 is ablated. Altogether, these *in vivo* data support a beneficial role for Opantimirs in different myopathies associated with primary or secondary mitochondrial defects via increased Opa1 expression.

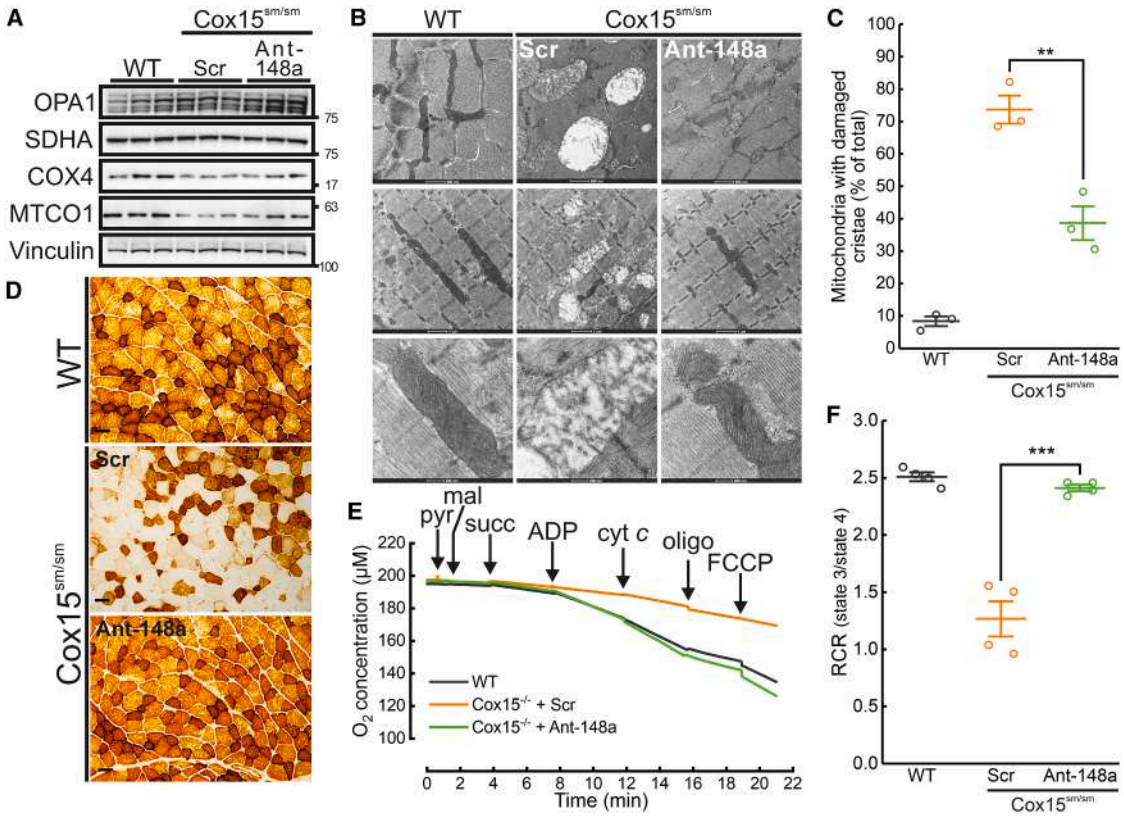

Figure 6. Opantimir148a restores mitochondrial ultrastructure and function in *Cox15*$^{sm/sm}$ mice

(A) Representative immunoblots from three individual mice of the indicated genotype treated with the indicated AntagomiR (6 pmol/injection) triweekly for 4 weeks by intramuscular (IM) injection at 3 different locations in the gastrocnemius. Muscle tissues were lysed, and equal amounts of lysates (15 μg) were separated by SDS-PAGE and immunoblotted using the indicated antibodies.

(B) Representative electron micrographs of gastrocnemii of the indicated genotype treated as indicated following the same protocol as in (A). Scale bar, 500 nm (top), 1,000 nm (middle), and 200 nm (bottom).

(C) Average ± SEM of the percentage of abnormal mitochondrial cristae in morphometric analyses from experiments as in (B) (n = 3 biological replicates). $^{**}p < 0.01$ in a one-way ANOVA.

(D) Representative images of cross sections of gastrocnemii stained for COX activity from mice of the indicated genotype treated in the same protocol as in (A). Scale bar, 40 μm.

(E) Representative traces of oxygen consumption of homogenized muscle tissue of the indicated genotype treated where indicated as in (A).

(F) Average ± SEM of 4 respiratory control ratio (state 3/state 4) measurements from individual mice in experiments as in (E) (N = 4 biological replicates). $^{***}p < 0.001$ in a one-way ANOVA.

In (C) and (F), each dot represents an individual mouse.

DISCUSSION

The crista-sculpting protein OPA1 represents a promising therapeutic target for tackling mitochondrial myopathies. Here, we uncover four candidate miRNAs (miR-148/152-3p family and miR-128-3p) that specifically regulate OPA1 expression levels in mammals. Because miR-148a-3p and miR-152-3p accumulate in patient-derived cell lines and mouse models of mitochondrial myopathies, blocking their action by Opantimirs, AntimiRs for the OPA1-miRNA, rescues mitochondrial ultrastructure and function and improves muscle function *in vivo* by selectively targeting the affected tissue. Our results demonstrate that a rationally designed biopharmaceutical therapy boosting Opa1 levels selectively in the skeletal muscle can ameliorate mitochondrial myopathies, offering a proof-of-principle therapy for mitochondrial disorders where Opa1 is dysregulated.

While genetic, constitutive upregulation of Opa1 levels can correct different models of mitochondrial disease[13,38] and Opa1 gene delivery protects dopaminergic neurons from mitochondrial toxins,[39] the first approach is clearly clinically impossible and the second not devoid of potential side effects. Moreover, uncontrolled Opa1 expression can be per se detrimental, as evidenced by the reported upregulation of Opa1 in several types of cancer.[40–43] Thus, a rational approach for a therapy based on Opa1-mediated correction of mitochondrial ultrastructural and functional defects in mitochondrial myopathies requires the identification of the drivers of Opa1 loss in these diseases. We searched multiple databases for miRNAs that were predicted to regulate Opa1 and upregulated in muscle

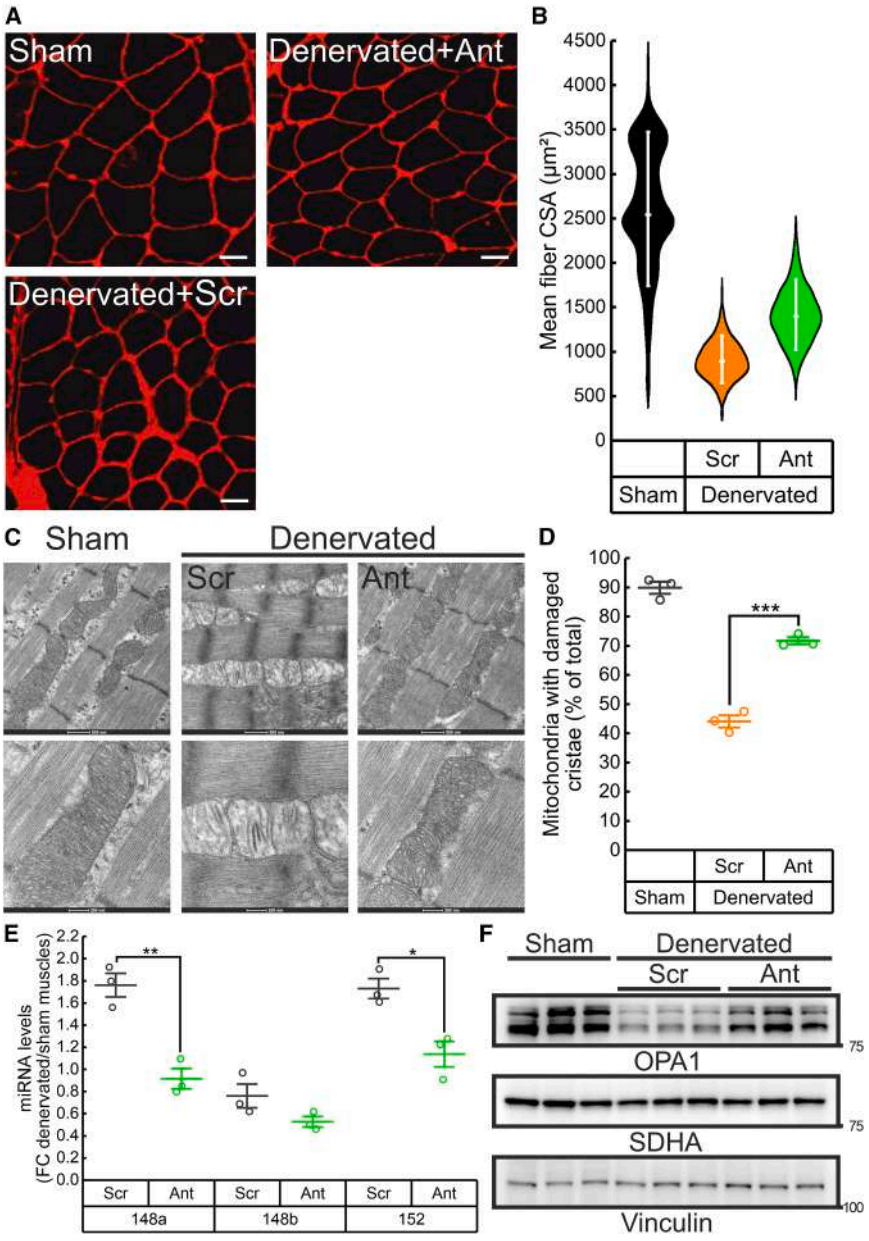

Figure 7. Opantimirs148a/152 protect muscles from sciatic neurectomy-induced atrophy

(A) Representative confocal images of cross sections of WGA-stained gastrocnemii from mice operated as indicated and treated with the indicated AntagomiR (6 pmol/injection) triweekly for 2 weeks by IM injection at 3 different locations in the gastrocnemius. Scale bar, 50 µm.

(B) Violin plots of fiber cross-sectional area from 3 biological replicate experiments as in (A). Median and 10th and 90th percentiles (whiskers) are shown. ****$p < 0.0001$ in a one-way ANOVA.

(C) Representative electron micrographs of gastrocnemii from experiments as in (A). Scale bar, 500 nm (top) and 200 nm (bottom).

(D) Average ± SEM of the percentage of mitochondria with abnormal cristae in morphometric analyses from experiments as in (C) ($N = 3$ biological replicates). ***$p < 0.001$ in a one-way ANOVA.

(E) Average ± SEM of expression levels by reverse-transcription PCR (RT-PCR) of the indicated miRNAs in gastrocnemii from experiments as (A) ($N = 3$ biological replicates). *$p < 0.05$ and **$p < 0.01$ in a Student's unpaired t test.

(F) In experiments as in (A), gastrocnemii were lysed and equal amounts of proteins (20 µg) were separated by SDS-PAGE and immunoblotted using the indicated antibodies. Each lane corresponds to an individual mouse.

diseases. This approach was successful in identifying the miR-148/152-3p family and miR-128-3p as both directly interacting with the 3 UTR region of Opa1 to regulate its expression and being upregulated in multiple muscle disorders such as Duchenne and facioscapulohumeral and limb-girdle muscular dystrophies[19,21] and in mouse models of muscle atrophy.[17] Additionally, we found miR-152-3p increased in *SURF1* patient cells, miR-148a-3p elevated in *Cox15*$^{sm/sm}$ mice, and miR-148a-3p and miR-152-3p levels induced in muscles 14 days post-sciatic neurectomy, negatively correlating with OPA1 levels. Our results establish that miR-148a-3p and miR-152-3p are implicated in mitochondrial myopathy and the atrophy program.

The miR-148/152-3p family and miR-128-3p are predominantly known for their tumor-suppressive roles in cancer.[44–46] In breast cancer cells, miR-148/152-3p family are epistatic to *OPA1*, their levels increasing upon OPA1 ablation and mediating OPA1-dependent inhibition of tumor growth and invasion.[42] *Cox15*$^{sm/sm}$ mice resemble a progressive mitochondrial myopathy featuring diminished muscle strength and size.[26] The biochemical outcome of the *Cox15* mutant allele is partial COX activity resulting in defective OXPHOS,[26] recapitulating the phenotype reported in human patients harboring *COX15* mutations.[27–29,47] Genetic overexpression of OPA1 mitigates denervation-induced muscle atrophy and ameliorates *Cox15*$^{sm/sm}$ mice, by correcting crista shape and recovering mitochondrial function.[12,13] However, genetically modified animals overexpressing OPA1 from birth do not accurately reflect a real disease setting, and the myopathy likely incompletely manifests. In our work, the delivery via triweekly intramuscular injections of specific AntimiRs that increase OPA1 levels in 6-week-old *Cox15*$^{sm/sm}$ mice, at a stage when muscle pathology is apparent, can inhibit the action of miR-148a-3p, increase OPA1 protein levels, correct mitochondrial ultrastructure, and importantly improve muscle function.

Developing pharmacological interventions for mitochondrial myopathy remains a challenge. Tested therapeutic compounds for mitochondrial myopathy include the antioxidants coenzyme

Q10 and its synthetic analog idebenone[4]; bezafibrate, a pan-peroxisome proliferator-activated receptor (PPAR) agonist that stimulates mitochondrial biogenesis[4]; and niacin that boosts nicotinamide adenine dinucleotide $(NAD)^+$ levels improving muscle function in mitochondrial myopathy patients.[5] Our current study offers a pharmacological approach involving a miRNA-based therapy that targets the OPA1-dependent crista remodeling pathway, independently of the underlying genetic cause of the mitochondrial disorder. In addition to mitochondrial disorders, miR-152-3p is also upregulated in primary open-angle glaucoma (POAG),[48] the leading cause of blindness with limited treatment options. In a recent large metanalysis, the rs166850 C/T and rs10451941T/C *OPA1* polymorphisms appeared significantly associated with the development of POAG, especially in Caucasian individuals.[49] Albeit it is unclear whether this polymorphism results in reduced Opa1 levels, the potential genetic and miRNA association points to *OPA1* as a factor in POAG development and to the AntagomiR 152-3p described here as a potential therapeutic strategy for this frequent neurodegenerative condition. Furthermore, mitochondrial ultrastructure is known to be altered in conditions such as heart failure where levels of Opa1 diminish.[50] Indeed, upon heart ischemia/reperfusion, Opa1 levels decrease, and its overexpression can prevent mitochondrial and tissue damage.[12] Notably, miR-152-3p levels increase in heart failure, and a transgenic model of miR-152-3p upregulation reproduces the mitochondrial ultrastructural derangements observed upon Opa1 downregulation. These changes, as well as heart function, are preserved by an AntagomiR targeting miR-152-3p,[51] indicating that Opantimirs might also be useful to treat heart failure. The miRNAs identified in our work can serve not only as an effective therapeutic target but also to track disease severity in mitochondrial myopathy. Because miR-148a-3p accumulated in *Cox15*$^{sm/sm}$ blood plasma and correlated with levels in muscle, monitoring plasma miRNA levels could be used as a means to bypass invasive muscle biopsies for use as a prognostic biomarker for mitochondrial myopathy.

ER stress levels influenced miR-148a-3p and miR-152-3p activity, and thus we speculate that ER stress transcription factors regulate miR-148a-3p and miR-152-3p expression in mitochondrial myopathy. Interestingly, ER stress transcription factor XBP1s was reported to directly modulate miR-148a-3p transcription.[52] We found that XBP1s mRNA levels correlated with miR-148a-3p levels in COX-deficient cells and tunicamycin-treated myotubes, hinting that XBP1s could be a specific regulator of miR-148a-3p expression. Future work should address the role of a potential XBP1s-miR-148a-3p-OPA1 circuit in mitochondrial myopathy to better understand the molecular mechanisms underlying the pathology.

Here, an AntimiR-based treatment was effective at increasing OPA1 expression levels and improving the phenotype in mitochondrial myopathies. Our work highlights Opa1 stabilization by miRNA therapy as a strategy against mitochondrial disorders.

Limitations of the study

Given the multifunctional nature of miRNAs, we cannot exclude the possibility that other factors regulated by miR-148/152 expression contributed to the phenotypic improvements observed in the myopathy models used in this study. However, our combined genetic approaches, genomic Opa1 deletion *in vitro* and *in vivo*, suggest that these miRNAs modulate mitochondrial ultrastructure, morphology, and function and muscle fiber size through endogenous Opa1 modulation. In this study, *in vitro* experiments demonstrated that ER stress influenced the activity of these miRNAs. However, whether this also occurs *in vivo* remains untested and warrants future investigation.

RESOURCE AVAILABILITY

Lead contact

Requests for further information should be directed to and will be fulfilled by the lead contact, Luca Scorrano (luca.scorrano@unipd.it).

Materials availability

All unique/stable reagents generated in this study are available from the lead contact with a completed materials transfer agreement.

Data and code availability

- The original data and uncropped western blots used to generate figures are included in Data S1 ZIP archive. The data used to generate Figure 1A are publicly available from GEO: GSE51648,[17] from the HMDD Database[18] (http://www.cuilab.cn/hmdd), and from Eisenberg et al.[19]
- This paper does not report original code.
- Any additional information required to reanalyze the data reported in this paper is available from the lead contact upon request.

ACKNOWLEDGMENTS

We thank Drs. F. Caicci and F. Boldrin (Bioimaging Facility, Department of Biology, University of Padova) for EM samples preparation and A. Cabrelle (FACS facility, VIMM) for flow cytometry. We thank Dr. P. Pecina (the Czech Academy of Sciences) for COX4I1 KO HEK293 cells and Dr. N. Surdo (VIMM) for helpful discussions. The graphical schematic was created using BioRender (BioRender.com). This study was supported by European Research Council ERC GA282280; Muscular Dystrophy Association 603731; AFM-Téléthon RG22326; Ministero dell'Istruzione, dell'Università e della Ricerca RBAP11Z3YA_005, PRIN 2017BF3PXZ; Ministero dell'Università e della Ricerca PRIN 2020PKLEPN_002 (L.S.); European Union-Next Generation EU, Mission 4, Component 2, CUP B93D21010860004 (L.S. and C.V.), and Mission 4, Component 2, Investment 1.2, MSCA_0000019; and MUR Concession Decree No. n. 564 CUP C93C22007550006 (L.A.). T.B.F. was the recipient of an AIRC postdoctoral fellowship; K.T. was supported by an EMBO postdoctoral fellowship and a Uehara Memorial Foundation postdoctoral fellowship.

AUTHOR CONTRIBUTIONS

Conceptualization: A.D., K.T., F.G., and L.S.; investigation: A.D., K.T., F.G., T. B.F., H.F., L.N., C. Barison, S.S., M.S., A.O., R.C., D.S., L.T., L.A., and C. Bean; visualization: A.D., K.T., F.G., T.B.F., H.F., L.N., C. Barison, S.S., M.S., A.O., R. C., D.S., L.T., L.A., C. Bean, C.V., B.B., and L.S.; funding acquisition: L.A., T.B. F., C.V., B.B., and L.S.; project administration: L.S.; supervision: C.V., B.B., and L.S.; writing – original draft: A.D. and L.S.; writing – review and editing: all authors.

DECLARATION OF INTERESTS

The authors declare no competing interests.

STAR★METHODS

Detailed methods are provided in the online version of this paper and include the following:

- KEY RESOURCES TABLE
- EXPERIMENTAL MODEL AND STUDY PARTICIPANT DETAILS
  - Mouse models
  - Animal handling and maintenance
  - Mouse adult fibroblast generation
  - Cell culture
- METHOD DETAILS
  - Intramuscular drug delivery
  - Sciatic nerve denervation
  - Blood analysis
  - Transfection
  - Western blotting
  - RNA isolation and gene expression analyses
  - Plasmids and molecular biology
  - Dual-luciferase reporter assay
  - Adenovirus infection
  - Confocal microscopy
  - Cell proliferation and viability assay
  - Transmission electron microscopy
  - Morphological analysis
  - Oxygen consumption measurements
  - Muscle force measurements
- QUANTIFICATION AND STATISTICAL ANALYSIS

SUPPLEMENTAL INFORMATION

Supplemental information can be found online at https://doi.org/10.1016/j.xcrm.2025.102248.

Received: November 13, 2024
Revised: April 18, 2025
Accepted: June 27, 2025
Published: July 24, 2025

REFERENCES

1. Gorman, G.S., Chinnery, P.F., DiMauro, S., Hirano, M., Koga, Y., McFarland, R., Suomalainen, A., Thorburn, D.R., Zeviani, M., and Turnbull, D. M. (2016). Mitochondrial diseases. Nat. Rev. Dis. Primers *2*, 16080. https://doi.org/10.1038/nrdp.2016.80.
2. Suomalainen, A., and Battersby, B.J. (2018). Mitochondrial diseases: the contribution of organelle stress responses to pathology. Nat. Rev. Mol. Cell Biol. *19*, 77–92. https://doi.org/10.1038/nrm.2017.66.
3. Ghezzi, D., and Zeviani, M. (2018). Human diseases associated with defects in assembly of OXPHOS complexes. Essays Biochem. *62*, 271–286. https://doi.org/10.1042/EBC20170099.
4. Ahmed, S.T., Craven, L., Russell, O.M., Turnbull, D.M., and Vincent, A.E. (2018). Diagnosis and Treatment of Mitochondrial Myopathies. Neurotherapeutics *15*, 943–953. https://doi.org/10.1007/s13311-018-00674-4.
5. Pirinen, E., Auranen, M., Khan, N.A., Brilhante, V., Urho, N., Pessia, A., Hakkarainen, A., Ulla Heinonen, J.K., Schmidt, M.S., Haimilahti, K., et al. (2020). Niacin Cures Systemic NAD(+) Deficiency and Improves Muscle Performance in Adult-Onset Mitochondrial Myopathy. Cell Metab. *32*, 144. https://doi.org/10.1016/j.cmet.2020.05.020.
6. Vincent, A.E., Ng, Y.S., White, K., Davey, T., Mannella, C., Falkous, G., Feeney, C., Schaefer, A.M., McFarland, R., Gorman, G.S., et al. (2016). The Spectrum of Mitochondrial Ultrastructural Defects in Mitochondrial Myopathy. Sci. Rep. *6*, 30610. https://doi.org/10.1038/srep30610.
7. Quintana-Cabrera, R., and Scorrano, L. (2023). Determinants and outcomes of mitochondrial dynamics. Mol. Cell *83*, 857–876. https://doi.org/10.1016/j.molcel.2023.02.012.
8. Giacomello, M., Pyakurel, A., Glytsou, C., and Scorrano, L. (2020). The cell biology of mitochondrial membrane dynamics. Nat. Rev. Mol. Cell Biol. *21*, 204–224. https://doi.org/10.1038/s41580-020-0210-7.
9. Tilokani, L., Nagashima, S., Paupe, V., and Prudent, J. (2018). Mitochondrial dynamics: overview of molecular mechanisms. Essays Biochem. *62*, 341–360. https://doi.org/10.1042/EBC20170104.
10. Djalalvandi, A., and Scorrano, L. (2022). Mitochondrial dynamics: roles in exercise physiology and muscle mass regulation. Curr. Opin. Physiol. *27*, 100550.
11. Tezze, C., Romanello, V., Desbats, M.A., Fadini, G.P., Albiero, M., Favaro, G., Ciciliot, S., Soriano, M.E., Morbidoni, V., Cerqua, C., et al. (2017). Age-Associated Loss of OPA1 in Muscle Impacts Muscle Mass, Metabolic Homeostasis, Systemic Inflammation, and Epithelial Senescence. Cell Metab. *25*, 1374–1389.e6. https://doi.org/10.1016/j.cmet.2017.04.021.
12. Varanita, T., Soriano, M.E., Romanello, V., Zaglia, T., Quintana-Cabrera, R., Semenzato, M., Menabò, R., Costa, V., Civiletto, G., Pesce, P., et al. (2015). The OPA1-dependent mitochondrial cristae remodeling pathway controls atrophic, apoptotic, and ischemic tissue damage. Cell Metab. *21*, 834–844. https://doi.org/10.1016/j.cmet.2015.05.007.
13. Civiletto, G., Varanita, T., Cerutti, R., Gorletta, T., Barbaro, S., Marchet, S., Lamperti, C., Viscomi, C., Scorrano, L., and Zeviani, M. (2015). Opa1 overexpression ameliorates the phenotype of two mitochondrial disease mouse models. Cell Metab. *21*, 845–854. https://doi.org/10.1016/j.cmet.2015.04.016.
14. Bartel, D.P. (2018). Metazoan MicroRNAs. Cell *173*, 20–51. https://doi.org/10.1016/j.cell.2018.03.006.
15. Krutzfeldt, J., Rajewsky, N., Braich, R., Rajeev, K.G., Tuschl, T., Manoharan, M., and Stoffel, M. (2005). Silencing of microRNAs in vivo with 'antagomirs. Nature *438*, 685–689. https://doi.org/10.1038/nature04303.
16. Lennox, K.A., and Behlke, M.A. (2011). Chemical modification and design of anti-miRNA oligonucleotides. Gene Ther. *18*, 1111–1120. https://doi.org/10.1038/gt.2011.100.
17. Soares, R.J., Cagnin, S., Chemello, F., Silvestrin, M., Musaro, A., De Pitta, C., Lanfranchi, G., and Sandri, M. (2014). Involvement of microRNAs in the regulation of muscle wasting during catabolic conditions. J. Biol. Chem. *289*, 21909–21925. https://doi.org/10.1074/jbc.M114.561845.
18. Cui, C., Zhong, B., Fan, R., and Cui, Q. (2024). HMDD v4.0: a database for experimentally supported human microRNA-disease associations. Nucleic Acids Res. *52*, D1327–D1332. https://doi.org/10.1093/nar/gkad717.
19. Eisenberg, I., Eran, A., Nishino, I., Moggio, M., Lamperti, C., Amato, A.A., Lidov, H.G., Kang, P.B., North, K.N., Mitrani-Rosenbaum, S., et al. (2007). Distinctive patterns of microRNA expression in primary muscular disorders. Proc. Natl. Acad. Sci. USA *104*, 17016–17021. https://doi.org/10.1073/pnas.0708115104.
20. Herkenne, S., Ek, O., Zamberlan, M., Pellattiero, A., Chergova, M., Chivite, I., Novotná, E., Rigoni, G., Fonseca, T.B., Samardzic, D., et al. (2020). Developmental and Tumor Angiogenesis Requires the Mitochondria-Shaping Protein Opa1. Cell Metab. *31*, 987–1003.e8. https://doi.org/10.1016/j.cmet.2020.04.007.
21. Dmitriev, P., Stankevicins, L., Ansseau, E., Petrov, A., Barat, A., Dessen, P., Robert, T., Turki, A., Lazar, V., Labourer, E., et al. (2013). Defective regulation of microRNA target genes in myoblasts from facioscapulohumeral dystrophy patients. J. Biol. Chem. *288*, 34989–35002. https://doi.org/10.1074/jbc.M113.504522.
22. Sue, C.M., Karadimas, C., Checcarelli, N., Tanji, K., Papadopoulou, L.C., Pallotti, F., Guo, F.L., Shanske, S., Hirano, M., De Vivo, D.C., et al. (2000).

Differential features of patients with mutations in two COX assembly genes, SURF-1 and SCO2. Ann. Neurol. *47*, 589–595.

23. van Riesen, A.K.J., Antonicka, H., Ohlenbusch, A., Shoubridge, E.A., and Wilichowski, E.K.G. (2006). Maternal segmental disomy in Leigh syndrome with cytochrome c oxidase deficiency caused by homozygous SURF1 mutation. Neuropediatrics *37*, 88–94. https://doi.org/10.1055/s-2006-924227.
24. Martinez Lyons, A., Ardissone, A., Reyes, A., Robinson, A.J., Moroni, I., Ghezzi, D., Fernandez-Vizarra, E., and Zeviani, M. (2016). COA7 (C1orf163/RESA1) mutations associated with mitochondrial leukoencephalopathy and cytochrome c oxidase deficiency. J. Med. Genet. *53*, 846–849. https://doi.org/10.1136/jmedgenet-2016-104194.
25. Melchionda, L., Haack, T.B., Hardy, S., Abbink, T.E.M., Fernandez-Vizarra, E., Lamantea, E., Marchet, S., Morandi, L., Moggio, M., Carrozzo, R., et al. (2014). Mutations in APOPT1, encoding a mitochondrial protein, cause cavitating leukoencephalopathy with cytochrome c oxidase deficiency. Am. J. Hum. Genet. *95*, 315–325. https://doi.org/10.1016/j.ajhg.2014.08.003.
26. Viscomi, C., Bottani, E., Civiletto, G., Cerutti, R., Moggio, M., Fagiolari, G., Schon, E.A., Lamperti, C., and Zeviani, M. (2011). In vivo correction of COX deficiency by activation of the AMPK/PGC-1alpha axis. Cell Metab. *14*, 80–90. https://doi.org/10.1016/j.cmet.2011.04.011.
27. Alfadhel, M., Lillquist, Y.P., Waters, P.J., Sinclair, G., Struys, E., McFadden, D., Hendson, G., Hyams, L., Shoffner, J., and Vallance, H.D. (2011). Infantile cardioencephalopathy due to a COX15 gene defect: report and review. Am. J. Med. Genet. *155A*, 840–844. https://doi.org/10.1002/ajmg.a.33881.
28. Antonicka, H., Mattman, A., Carlson, C.G., Glerum, D.M., Hoffbuhr, K.C., Leary, S.C., Kennaway, N.G., and Shoubridge, E.A. (2003). Mutations in COX15 produce a defect in the mitochondrial heme biosynthetic pathway, causing early-onset fatal hypertrophic cardiomyopathy. Am. J. Hum. Genet. *72*, 101–114. https://doi.org/10.1086/345489.
29. Bugiani, M., Tiranti, V., Farina, L., Uziel, G., and Zeviani, M. (2005). Novel mutations in COX15 in a long surviving Leigh syndrome patient with cytochrome c oxidase deficiency. J. Med. Genet. *42*, e28. https://doi.org/10.1136/jmg.2004.029926.
30. Debattisti, V., Pendin, D., Ziviani, E., Daga, A., and Scorrano, L. (2014). Reduction of endoplasmic reticulum stress attenuates the defects caused by Drosophila mitofusin depletion. J. Cell Biol. *204*, 303–312. https://doi.org/10.1083/jcb.201306121.
31. Kaspar, S., Oertlin, C., Szczepanowska, K., Kukat, A., Senft, K., Lucas, C., Brodesser, S., Hatzoglou, M., Larsson, O., Topisirovic, I., and Trifunovic, A. (2021). Adaptation to mitochondrial stress requires CHOP-directed tuning of ISR. Sci. Adv. *7*, eabf0971. https://doi.org/10.1126/sciadv.abf0971.
32. Maurel, M., and Chevet, E. (2013). Endoplasmic reticulum stress signaling: the microRNA connection. Am. J. Physiol. Cell Physiol. *304*, C1117–C1126. https://doi.org/10.1152/ajpcell.00061.2013.
33. Abu-Libdeh, B., Douiev, L., Amro, S., Shahrour, M., Ta-Shma, A., Miller, C., Elpeleg, O., and Saada, A. (2017). Mutation in the COX4I1 gene is associated with short stature, poor weight gain and increased chromosomal breaks, simulating Fanconi anemia. Eur. J. Hum. Genet. *25*, 1142–1146. https://doi.org/10.1038/ejhg.2017.112.
34. Quéméner-Redon, S., Bénech, C., Audebert-Bellanger, S., Friocourt, G., Planes, M., Parent, P., and Férec, C. (2013). A small de novo 16q24.1 duplication in a woman with severe clinical features. Eur. J. Med. Genet. *56*, 211–215. https://doi.org/10.1016/j.ejmg.2013.01.001.
35. Scorrano, L., Oakes, S.A., Opferman, J.T., Cheng, E.H., Sorcinelli, M.D., Pozzan, T., and Korsmeyer, S.J. (2003). BAX and BAK regulation of endoplasmic reticulum Ca2+: a control point for apoptosis. Science *300*, 135–139. https://doi.org/10.1126/science.1081208.
36. Germani, S., Van Ho, A.T., Cherubini, A., Varone, E., Chernorudskiy, A., Renna, G.M., Fumagalli, S., Gobbi, M., Lucchetti, J., Bolis, M., et al. (2024). SEPN1-related myopathy depends on the oxidoreductase ERO1A and is druggable with the chemical chaperone TUDCA. Cell Rep. Med. *5*, 101439. https://doi.org/10.1016/j.xcrm.2024.101439.
37. Li, Z., and Rana, T.M. (2014). Therapeutic targeting of microRNAs: current status and future challenges. Nat. Rev. Drug Discov. *13*, 622–638. https://doi.org/10.1038/nrd4359.
38. Luna-Sanchez, M., Benincá, C., Cerutti, R., Brea-Calvo, G., Yeates, A., Scorrano, L., Zeviani, M., and Viscomi, C. (2020). Opa1 Overexpression Protects from Early-Onset Mpv17(-/-)-Related Mouse Kidney Disease. Mol. Ther. *28*, 1918–1930. https://doi.org/10.1016/j.ymthe.2020.06.010.
39. Ramonet, D., Perier, C., Recasens, A., Dehay, B., Bové, J., Costa, V., Scorrano, L., and Vila, M. (2013). Optic atrophy 1 mediates mitochondria remodeling and dopaminergic neurodegeneration linked to complex I deficiency. Cell Death Differ. *20*, 77–85. https://doi.org/10.1038/cdd.2012.95.
40. Baek, M.L., Lee, J., Pendleton, K.E., Berner, M.J., Goff, E.B., Tan, L., Martinez, S.A., Mahmud, I., Wang, T., Meyer, M.D., et al. (2023). Mitochondrial structure and function adaptation in residual triple negative breast cancer cells surviving chemotherapy treatment. Oncogene *42*, 1117–1131. https://doi.org/10.1038/s41388-023-02596-8.
41. Larrue, C., Mouche, S., Lin, S., Simonetta, F., Scheidegger, N.K., Poulain, L., Birsen, R., Sarry, J.E., Stegmaier, K., and Tamburini, J. (2023). Mitochondrial fusion is a therapeutic vulnerability of acute myeloid leukemia. Leukemia *37*, 765–775. https://doi.org/10.1038/s41375-023-01835-x.
42. Zamberlan, M., Boeckx, A., Muller, F., Vinelli, F., Ek, O., Vianello, C., Coart, E., Shibata, K., Christian, A., Grespi, F., et al. (2022). Inhibition of the mitochondrial protein Opa1 curtails breast cancer growth. J. Exp. Clin. Cancer Res. *41*, 95. https://doi.org/10.1186/s13046-022-02304-6.
43. Chen, X., Glytsou, C., Zhou, H., Narang, S., Reyna, D.E., Lopez, A., Sakellaropoulos, T., Gong, Y., Kloetgen, A., Yap, Y.S., et al. (2019). Targeting Mitochondrial Structure Sensitizes Acute Myeloid Leukemia to Venetoclax Treatment. Cancer Discov. *9*, 890–909. https://doi.org/10.1158/2159-8290.Cd-19-0117.
44. Chen, Y., Song, Y.X., and Wang, Z.N. (2013). The microRNA-148/152 family: multi-faceted players. Mol. Cancer *12*, 43. https://doi.org/10.1186/1476-4598-12-43.
45. Liu, X., Li, J., Qin, F., and Dai, S. (2016). miR-152 as a tumor suppressor microRNA: Target recognition and regulation in cancer. Oncol. Lett. *11*, 3911–3916. https://doi.org/10.3892/ol.2016.4509.
46. Xu, Y., Chen, B., George, S.K., and Liu, B. (2015). Downregulation of MicroRNA-152 contributes to high expression of DKK1 in multiple myeloma. RNA Biol. *12*, 1314–1322. https://doi.org/10.1080/15476286.2015.1094600.
47. Galvao de Oliveira, M., Tengan, C., Micheletti, C., Ramos de Macedo, P., Soares Pinho Cernach, M.C., Cavole, T.R., de Franca Basto, M., Filho, J. S., Virmond, L.A., Milanezi, F., et al. (2021). A novel variant in the COX15 gene causing a fatal infantile cardioencephalomyopathy: A case report with clinical and molecular review. Eur. J. Med. Genet. *64*, 104195. https://doi.org/10.1016/j.ejmg.2021.104195.
48. Pinazo-Durán, M.D., Zanón-Moreno, V., García-Villanueva, C., Martucci, A., Peris-Martínez, C., Vila-Arteaga, J., García-Medina, J.J., Andrés-Blasco, I., Gallego-Martínez, A., Nucci, C., and García-Feijoo, J. (2023). Biochemical-molecular-genetic biomarkers in the tear film, aqueous humor, and blood of primary open-angle glaucoma patients. Front. Med. *10*, 1157773. https://doi.org/10.3389/fmed.2023.1157773.
49. Liu, Y.F., Luo, X.Y., Zhao, Z.C., Zheng, W., Lv, H.Y., and Luo, W.M. (2024). Association between optic atrophy 1 polymorphisms and primary open angle glaucoma risk: Based on a meta-analysis. Eur. J. Ophthalmol. *34*, 708–718. https://doi.org/10.1177/11206721231208244.
50. Chen, L., Gong, Q., Stice, J.P., and Knowlton, A.A. (2009). Mitochondrial OPA1, apoptosis, and heart failure. Cardiovasc. Res. *84*, 91–99. https://doi.org/10.1093/cvr/cvp181.

51. LaRocca, T.J., Seeger, T., Prado, M., Perea-Gil, I., Neofytou, E., Mecham, B.H., Ameen, M., Chang, A.C.Y., Pandey, G., Wu, J.C., and Karakikes, I. (2020). Pharmacological Silencing of MicroRNA-152 Prevents Pressure Overload–Induced Heart Failure. Circ. Heart Fail. *13*, e006298. https://doi.org/10.1161/CIRCHEARTFAILURE.119.006298.

52. Cho, Y.M., Kim, T.M., Hun Kim, D., Hee Kim, D., Jeong, S.W., and Kwon, O.J. (2016). miR-148a is a downstream effector of X-box-binding protein 1 that silences Wnt10b during adipogenesis of 3T3-L1 cells. Exp. Mol. Med. *48*, e226. https://doi.org/10.1038/emm.2016.3.

53. Cogliati, S., Frezza, C., Soriano, M.E., Varanita, T., Quintana-Cabrera, R., Corrado, M., Cipolat, S., Costa, V., Casarin, A., Gomes, L.C., et al. (2013). Mitochondrial cristae shape determines respiratory chain supercomplexes assembly and respiratory efficiency. Cell *155*, 160–171. https://doi.org/10.1016/j.cell.2013.08.032.

54. Sciacco, M., and Bonilla, E. (1996). Cytochemistry and immunocytochemistry of mitochondria in tissue sections. Methods Enzymol. *264*, 509–521.

STAR★METHODS

KEY RESOURCES TABLE

REAGENT or RESOURCE	SOURCE	IDENTIFIER
Antibodies		
Anti-OPA1 mouse	BD Biosciences (1:2000)	Cat#612607; RRID:AB_399889
Anti-TOM40 rabbit	Santa Cruz Biotechnology (1:1000)	Cat#ab185543; RRID:AB_3095412
Anti-Vinculin mouse	Abcam (1:10 000)	Cat#ab219649; RRID:AB_2819348
Anti-SDHA mouse	Abcam (1:1000)	Cat#ab14715; RRID:AB_301433
Anti-COX4 rabbit	Cell Signaling (1:1000)	Cat#4850; RRID:AB_2085424
Anti-MT-CO1	Cell Signaling (1:1000)	Cat#62101; RRID:AB_3678687
Anti-MFN1 rabbit	Cell Signaling (1:1000)	Cat#14739; RRID:AB_2744531
Anti-MFN2 mouse	Abnova (1:1000)	Cat#H00009927-M03; RRID:AB_530127
Anti-DLP1 mouse	BD Transduction Laboratories (1:1000)	Cat#611113; RRID:AB_398424
Anti-MFF rabbit	Proteintech	Cat#17090-1-AP; RRID:AB_2142463
Anti-FIS1 rabbit	Proteintech	Cat#10956-1-AP; RRID:AB_2102532
Anti-OXPHOS cocktail mouse	Abcam (1:1000)	Cat#ab110412; RRID:AB_2847807
Chemicals, peptides, and recombinant proteins		
CCCP	Sigma-Aldrich	Cat#C2759
Actinonin	Sigma-Aldrich	Cat#A6671
Rotenone	Sigma-Aldrich	Cat#R8875
Antimycin	Sigma-Aldrich	Cat#A8674
Oligomycin	Sigma-Aldrich	Cat#75351
Tunicamycin	Sigma-Aldrich	Cat#T7765
TUDCA	Millipore	Cat#580549
Critical commercial assays		
Dual-Luciferase® Reporter Assay	Promega	Cat#E1910
iScript cDNA Kit	Bio-Rad	Cat#1708890
SYBR™ Green PCR Master Mix	Thermo Fisher Scientific	Cat#A25741
TaqMan™ Universal PCR Master Mix	Thermo Fisher Scientific	Cat#4304437
Pierce protein BCA assay	Thermo Fisher Scientific	Cat#23227
QuikChange II XL Site-Directed Mutagenesis Kit	Agilent Technologies	Cat#200521
Experimental models: Cell lines		
Opa1$^{fl/fl}$ MAF	This paper	N/A
Opa1$^{fl/fl}$::*Opa1*^{tg} MAF	This paper	N/A
Normal skin fibroblast	ATCC	Cat#PCS-201-012
SURF1 skin fibroblast	Telethon Biobank	mt4595
SURF1 skin fibroblast	Telethon Biobank	mt2979
APOPT1 skin fibroblast	Telethon Biobank	mt189
COA7 skin fibroblast	Telethon Biobank	*COA7*
Experimental models: Organisms/strains		
Cox15$^{sm/sm}$ mice	Civiletto et al.[26]	N/A
Opa1$^{sm/sm}$ mice	Tezze et al.[11]	N/A
Oligonucleotides		
mirVana miRNA mimic	Thermo Fisher Scientific	Cat#4464066
microDOWN AntagomiR	Creative Biogene	Cat#CBGAB0584-4
See Table S1 for oligonucleotide sequences	This paper	N/A

(*Continued on next page*)

Continued

REAGENT or RESOURCE	SOURCE	IDENTIFIER
Software and algorithms		
OriginPro V2024	OriginLab	https://www.originlab.com/
CorelDRAW Graphics Suite V2022	Corel	https://www.coreldraw.com/
ImageJ	NIH	https://imagej.nih.gov/ij/
Other		
DMEM	GIBCO	Cat#31885049
Penicillin-streptomycin (5000U/mL)	Invitrogen	Cat#15070-063
Trypsin-EDTA (0.25%)	Thermo Fisher Scientific	Cat#25200056
Bovine Serum Albumin	Sigma Aldrich	Cat#A8806
Amersham Hybond 0.45μm PVDF	Thermo Fisher Scientific	Cat#15407374
NuPAGE^{TM} 3 to 8% gel	Thermo Fisher Scientific	Cat#EA0375BOX

EXPERIMENTAL MODEL AND STUDY PARTICIPANT DETAILS

Mouse models

Animal housing and all the experimental procedures were authorized by the Italian Ministry of Health (approved protocols: 383-2015-PR; 564/2020-PR and 390/2024-PR to L.S.). Skeletal muscle-specific Cox15$^{-/-}$ mouse mice (Cox15$^{sm/sm}$) were generated by crossing Cox15$^{loxP/loxP}$ individuals with mice that express Cre recombinase under the control of the human skeletal muscle-specific α-actin (ACTA1) promoter.[26] Littermates of the same sex were randomly assigned to experimental groups. These mice were maintained on a mixed C57Bl6/129Sv genetic background.[26] The tamoxifen-inducible muscle-specific OPA1 knockout mice (Opa1$^{sm/sm}$, HAS-Cre-ER::*Opa1*$^{fl/fl}$) was previously described.[11] Tamoxifen diet was administered to 3-month-old male mice, with muscles collected 45 days after starting the diet. Cre-negative littermates treated with tamoxifen served as controls.

Animal handling and maintenance

Animals were handled by specialized personnel under the control of the Veterinary Service of the University of Padova and VIMM. Animals were maintained in a temperature (22°C) and humidity (60%) controlled animal-care facility with a 12 h light/dark cycle and free access to water and food and were sacrificed by cervical dislocation after 3.5% isoflurane anesthesia.

Mouse adult fibroblast generation

This procedure was carried out on diaphragm tissue from male C57BL/6J mice. The tissue was sectioned and transferred into a 15 mL Falcon tube containing 10 mL of pre-warmed, sterile digestion buffer (1 mg/mL collagenase II in DMEM supplemented with 20% FBS, 1% non-essential amino acids, and 1% penicillin/streptomycin). The sample was gently resuspended 10 times and incubated at 37°C in a water bath for 8 min. This digestion step was repeated twice. After each incubation, the supernatant was collected and kept on ice, fresh digestion buffer was added to the remaining tissue, and the resuspension/incubation sequence was performed as described. All supernatants were then pooled, filtered through a cell strainer, and centrifuged at 600 × g for 5 min. The resulting pellet was resuspended and plated into a six-well plate for overnight culture. After 24 h, the medium in each well was replaced with fresh culture medium.

Cell culture

MAFs and HEK293 cells were cultured in Dulbecco's Modified Medium (DMEM, Invitrogen) containing 4.5 mg/mL glucose and supplemented with 10% fetal bovine serum (FBS, Invitrogen), 2 mM L-glutamine, 50 U/ml penicillin, 50 μg/mL streptomycin (Invitrogen), 100 μM non-essential amino acids (Invitrogen) at 37°C and 5% CO_2 atmosphere. Patient-derived skin fibroblasts were cultured in Ham's F-12 nutrient mixture (F12 medium; Gibco) supplemented with 10% FBS and 1% penicillin-streptomycin (Thermo Fisher Scientific) at 37°C and 5% CO_2 atmosphere. C2C12 mouse myoblast cells were cultured in DMEM supplemented with 10% FBS and 1% penicillin-streptomycin (Invitrogen). at 37°C and 5% CO_2 atmosphere. For routine maintenance, cells were passaged at 70–80% confluency. To induce myogenic differentiation, growth medium was replaced with differentiation medium (DMEM supplemented with 2% horse serum and 1% penicillin-streptomycin) when cells reached 90% confluency. Differentiation medium was changed every 24h for 5-7 days to allow for myotube formation. Drugs were used at the following concentrations: CCCP 5 μM, actinonin 50 μM, oligomycin 1 mg/mL, tunicamycin 1 μg/mL and TUDCA 200 μM. Cells were not validated. Cells were tested for Mycoplasma every month by RT-PCR.

METHOD DETAILS

Intramuscular drug delivery

Mice were anesthetized by 3.5% isoflurane. AntimiR specific for miRNA mimics were resuspended in PBS at a final concentration of 100 nM. Mice were injected triweekly with an AntimiR mix or scramble control of at three distinct local injections (3 $\times$ 20 μL) in the gastrocnemius muscle.

Sciatic nerve denervation

Male 3–5-month-old C57BL/6 mice were randomly assigned to two experimental groups, scramble and AntimiR. Sham (non-denervated) leg of animals was used as the control. All mice were maintained under the same conditions. Mice were anesthetized by isoflurane and the sciatic nerve was excised and removed, followed by stitching up of the wounded area. Gastrocnemii of mice having undergone denervation were snap frozen and collected at 14days post denervation to be used for biochemical and morphological analysis.

Blood analysis

Blood was collected from mouse tail vein. Total blood count was analyzed using the CELL-DYN Emerald Hematology Analyzer (Abbott) on fresh EDTA-treated mouse blood.

Transfection

Transfection was performed using Lipofectamine RNAiMAX (Invitrogen) following the manufacturer's recommended protocol. For the procedure, cells were seeded in 6-well plates, with each well containing 3 x 10^5 cells. The transfection mixture was prepared by combining 30 nM of miRNA mimic or scramble mimic with the Lipofectamine reagent. This mixture was then added to cells, which were subsequently analyzed 48h post-transfection.

Western blotting

Cells were lysed in RIPA buffer (50 mM Tris-HCl, pH 7.4, 150 mM NaCl, 1% NP-40, 0.5% sodium deoxycholate, 0.1%SDS, 1 mM EDTA,1 mM EGTA) and heated at 95°C for 10 min. Protein samples of equivalent concentrations were then separated by 8% SDS-PAGE and transferred onto polyvinylidene fluoride (PVDF) membranes, adhering to the manufacturer's guidelines. Membrane blocking was performed at RT for 1 h, utilizing a 5% (w/v) Dried Skimmed Milk in tris-buffered saline with tween 0.5% Tween 20 (TBST) for 60 min at room. Primary antibody incubation occurred overnight at 4°C at a 1:1000 dilution. Following a series of three TBS-T washes, the membranes were exposed to the corresponding secondary antibody (1:2000 dilution) for 1 h at RT. Protein band visualization was achieved using an enhanced chemiluminescence (ECL) substrate (Thermo Fisher Scientific). Densitometric analysis was performed using ImageJ to quantify relative levels of protein bands.

RNA isolation and gene expression analyses

RNA isolation, reverse transcription and real time quantitative PCR

Total RNA from cells and muscle tissue was extracted using the TRIzol (Thermo Fisher Scientific) method according to the manufacturer's protocol. RNA quantity and quality were assessed using a Nanodrop One spectrophotometer (ThermoFisher), with purity evaluated by 260:280 and 260:230 nm absorbance ratios. Complementary DNA (cDNA) was synthesized using 1 μg RNA that was reverse transcribed using M-MLV Reverse Transcriptase (Bio-Rad) according to the manufacturer's protocol. cDNA used for quantitative RT-PCR reactions using SYBR Green PCR Master Mix reagents (Thermo Fisher Scientific) and performed using thermocycler in a 384-well plate. For normalization pan-actin was used as housekeeping gene. Gene expression changes were calculated using the $2^{(-\Delta\Delta CT)}$ method. Results are presented as fold changes in expression, normalized to reference gene expression.

miRNA expression analysis

Total RNA from cells and muscle tissue was extracted using TRIzol (Thermo Fisher Scientific) method according to the manufacturer's protocol. In a two-step process, RNA was reverse transcribed into complementary miRNA using miRNA-specific stem-loop primers (Thermo Fisher Scientific) for the miR-148/152-3p and miR-128-3p family and U6 was used as a housekeeping gene. Diluted miRNA template (10 ng/μL) was used for quantitative RT-PCR reactions using TaqMan chemistry (Thermo Fisher Scientific) and performed using a thermocycler in a 384-well plate. All data were normalized to U6 gene. Results were analyzed using the $2^{(-\Delta\Delta CT)}$ method. Results are presented as fold changes in expression, normalized to reference gene expression.

Plasmids and molecular biology

The psiCHECK-2 reporter vector used for luciferase-based experiments contained inserts of a two-repeat complementary sequence to the seed region of miR-148a-3p, miR-148b-3p, miR-152-3p and miR-128-3p, and a ~500bp fragment of mouse and human OPA1 3 UTR where miR-148/152-3p family and miR-128-3p target. Three substitution mutations were introduced into the miRNA response elements of OPA1 3 UTR-containing plasmids using a site-directed mutagenesis kit, following the manufacturer's instructions and using the primer sequences reported in Table S1. For the miR-148/152-specific OPA1 3 UTR fragment, nucleotides 3–5 were

changed from GTCACG to GAGTCG, and for the miR-128- specific OPA1 3 UTR, nucleotides 3–5 were changed from CACTGTG to CAGAGTG.

Dual-luciferase reporter assay

Dual-luciferase reporter system (Promega Corp) utilized the psiCHECK-2 vector that expressed Renilla luciferase (experimental) and Firefly luciferase (internal control) for bioluminescent signal detection. miRNA mimic inserts and OPA1 3 UTR fragments were placed downstream of Renilla. Cells were seeded at 0.5 x 10^4 cells per well in a 96-well plate, and 24h later, transfected with 0.1 μg of psiCHECK-2 using Lipofectamine 3000 (2:1 plasmid to reagent ratio). Cells were lysed in passive lysis buffer (30 μL). Ten μL of lysate was used for luminescence measurement: LARII (Firefly substrate) was added first, followed by Stop & Glo (Renilla substrate). The luminescence ratios of LARII to Stop & Glo were analyzed.

Adenovirus infection

Acute genomic *Opa1* depletion in *Opa1*$^{fl/fl}$::*Opa1*^{tg} MAFs was achieved through viral transduction. Specifically, adenoviruses expressing CRE-green fluorescent protein (GFP) (ad-CRE; Vector Biolabs) were used at a concentration of 300 pfu. As a control, adenoviruses expressing GFP alone (EV) were used at an equal titer.

Confocal microscopy

Cells were seeded at 0.4 x 10^5 cells per well in a 12-well on glass coverslips and treated as indicated. Next, cells were transfected with mitochondria-targeted red fluorescence protein (MitoRFP)-expressing plasmid for 48h and confocal images were acquired using a confocal microscope (Zeiss LSM900 Airyscan 2). The wavelengths of excitation and emission were 561 nm and 565–700 nm respectively. Mitochondrial branch length was analyzed using FIJI plugin MiNA.

Cell proliferation and viability assay

Crystal Violet staining (Sigma-Aldrich, C0775) was used to measure cell proliferation and viability. Cells were fixed at RT with 4% formaldehyde for 15 min, followed by PBS washes. Next, a 0.1% Crystal Violet solution was used to stain the cells for 20 min at RT. Post-staining, the cells were washed with Milli-Q H_2O before and dried overnight. Stained cells were lysed in 10% acetic acid with agitation for 30 min. Absorbance values were measured at 590 nm using a spectrophotometer.

Transmission electron microscopy

Cells underwent the treatment indicated, followed by fixation for 1 h at RT using 1.25% (v/v) glutaraldehyde in 0.1 M sodium-cacodylate at pH 7.2. Post-fixation, the samples were stored in 0.1 M sodium cacodylate buffer at 4°C. A Tecnai-20 electron microscope (Philips-FEI) was employed to image thin sections as described previously.[53]

Morphological analysis

All muscle tissues for morphological analysis were cut at 10 μM thin slices using a cryostat and imaged by a brightfield microscope (Leica CM1860UV). Sections were stained with hematoxylin and eosin reagents (Sigma-Aldrich) following the manufacturers protocol for histochemical examination. Sections for COX histochemical staining was performed as previously described.[54] For ultrastructural analysis, the samples were fixed in a solution of 2.5% glutaraldehyde in 10 mM PBS at pH 7.4. Samples were stored at 4°C in 0.1 M sodium cacodylate buffer until post fixation. Thin sections were imaged using Tecnai-20 electron microscope (Philips-FEI) as described.[53] For WGA-staining, sections were incubated with WGA (10 μg/mL) for 1 h at RT. After washing in PBS, sections were mounted with fluorescence mounting medium and visualized using Leica 6M6B microscope.

Oxygen consumption measurements

Skeletal muscle samples were collected and preserved in ice-cold BIOPS buffer (10 mM Ca-EGTA buffer, 0.1 μM free calcium, 20 mM imidazole, 20 mM taurine, 50 mM K-MES, 0.5 mM DTT, 6.56 mM MgCl2, 5.77 mM ATP, 15 mM phosphocreatine, pH 7.1). Samples were homogenized using a glass-on-glass homogenizer, then diluted to 2 mg/mL. High-resolution respirometry was performed using an Oroboros Oxygraph-2k high-resolution respirometer (Oroboros instruments) at 37°C in 2 mL chambers containing MiR06 mitochondrial respiration medium (MiR06; 0.5 mM EGTA, 3 mM $MgCl_2$, 60 mM lactobionic acid, 20 mM taurine, 10 mM KH_2PO_4, 20 mM HEPES, 110 mM sucrose, 1 g/L BSA, catalase 280 u/mL; pH 7.1). Oxygen concentration and flux were recorded in real-time using DatLab software. Homogenized sample (0.2 mg tissue) was added to chambers, followed by sequential additions of: glutamate/malate, succinate, ADP, cytochrome *c*, oligomycin and FCCP.

Muscle force measurements

Gastrocnemius muscle contractile performance was measured using a muscle lever system (1300A, Aurora Scientific). Mice were anesthetized with Xylazine and Zoletil, positioned on a temperature-controlled table with the knee stabilized and foot secured to a motor-connected footplate. Stainless-steel electrode wires were implanted on either side of the sciatic nerve to trigger contractions via electrical stimulation. To prevent dorsal flexor activation, the common peroneal nerve was severed. Isometric torque was recorded at increasing stimulation frequencies, with 30 s intervals to avoid fatigue, and eccentric contractions were performed by

moving the foot backward at 40 mm/s during tetanic stimulation (100 Hz). Force was calculated by dividing torque by the lever arm length (2.1 mm) and normalized to muscle mass to estimate relative force. After completing measurements, the mice were euthanized by cervical dislocation, and the muscles were dissected and weighed.

QUANTIFICATION AND STATISTICAL ANALYSIS

Experimental data from a minimum of three independent experiments are presented as dot plots. These plots display individual data points along with the mean and standard error of the mean (SEM). All figure legends include sample sizes (n) and *p* values. Statistical analysis was performed using OriginPro software (Microcal). Shapiro-Wilk test was employed to assess normal distribution of populations at a 0.05 significance level. To determine statistical significance for normally distributed data, Student's unpaired t test, one-way ANOVA and two-way ANOVA with Tukey's post-hoc test were used. For non-normally distributed data, Mann-Whitney U test and Kruskal–Wallis tests were applied. Data was considered statistically significant at $p \leq 0.05$ represented in figures by "*", where $^{*}p \leq 0.05$; $^{**}p \leq 0.01$; $^{***}p \leq 0.001$; $^{****}p \leq 0.0001$.